Engineering Structures 321 (2024) 118931

Contents lists available at ScienceDirect

Engineering Structures

journal homepage: www.elsevier.com/locate/engstruct

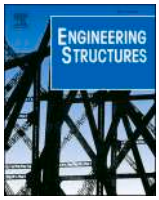

Review article

Post-necking and damage modelling of steel structural components: A comprehensive state of the art

Aldo Milone [a], Pietro Foti [b], Filippo Berto [b], Raffaele Landolfo [a,*]

[a] Department of Structures for Engineering and Architecture (DiST), University of Naples "Federico II", Via Forno Vecchio 36, Naples 80134, Italy
[b] Department of Chemical, Material and Environmental Engineering (DICMA), Sapienza University of Rome, via Eudossiana 18, Rome 00184, Italy

ARTICLE INFO

Keywords:
Structural Steels
Post-Necking Behaviour
Ductile Fracture
Finite Element Analysis

ABSTRACT

Numerical simulations are widely used both for research purposes and in technical practice to address structural design of steel components. When dealing with damage and ductile fracture of such components, the reliability of obtained outcomes strongly depend on adopting appropriate modelling assumptions. Nevertheless, up to very recent times, only few normative prescriptions were available for designers around the world regarding this topic, i.e., in spite of its strong implications in limit-state design of fracture-governed components (e.g., bolted connections, plates weakened by holes, etc…). In light of new developments of prEN1993–1-14:2023, which allows expert designers to implement advanced damage models for structural steel modelling, in the present work a review about consolidated formulations to capture post-necking and damage behaviour of steel components is presented, i.e., with the aim to serve as a guideline for either researchers and designers. To this end, on the basis of pioneering works and recent research contributions, the following topics are addressed: (*i*) post-necking behaviour of ductile structural steels, (*ii*) ductile damage initiation criteria and (*iii*) damage evolution criteria. Each presented formulation is critically reviewed based on notable applications drawn from literature. Finally, some examples of comprehensive use of such models for safety assessment of structural steel details are introduced and thoroughly discussed.

1. Introduction

Numerical modelling has become a crucial tool in several engineering fields, including structural design [1–6]. Currently, structural engineers typically address each phase of structural design (i.e., pre-dimensioning, iterative optimization, safety checks) through advanced numerical methods, with the finite element method (FEM) standing as the most popular option due to its general reliability, flexibility and diffusion in the form of plenty commercially available software [7–10].

Nevertheless, up to very recent times, very few or no systematic provisions or guidelines were available for designers around the world regarding the proper definition of modelling assumptions (i.e., boundary conditions, materials constitutive behaviour, mesh sizing, etc…), i.e., with some key choices being delegated to the lone expert judgment of the operator or, in worst cases, to the default settings of the FEM software. This can lead to gross errors in structural analysis and design [11,12].

With reference to steel structures and structural components, these normative gaps proved to be often crucial. Namely (*i*) in Europe, only few indications about FEM modelling were provided in single parts of EN1993 (e.g., EN1993–1-5 [13] covering plated structural elements or EN1993–1-6 [14] concerning the strength and stability of shell structures), i.e., with rules being heavy limited in their scope and leaving potential room for contradiction [15,16], and (*ii*) for American designers, although the use of FEM in structural design is explicitly allowed by ANSI/AISC 360–22 [17], very limited prescriptions are given in Appendix 1 of the same document – although few more indications about verification and validation of numerical models can be retrieved in ASME V&V10 [18] and AWS A9.5 [19] standards, i.e., with reference to plain and welded components, respectively.

For European countries, this impasse has been finally overcome within the framework of the M/515 EN mandate of the European Commission – "Mandate for amending existing Eurocodes and extending the scope of structural Eurocodes" [20] – which instructed the technical committee CEN/TC 250 to draft a second generation of Eurocodes incorporating all significant progresses in scientific research while aiming at solving key issues found in fifteen years of use of Eurocodes [21,22]. Among the several working groups (WGs), SC3/WG22

* Corresponding author.
E-mail addresses: aldo.milone@unina.it (A. Milone), pietro.foti@uniroma1.it (P. Foti), filippo.berto@uniroma1.it (F. Berto), landolfo@unina.it (R. Landolfo).

https://doi.org/10.1016/j.engstruct.2024.118931
Received 30 April 2024; Received in revised form 31 July 2024; Accepted 3 September 2024
Available online 11 September 2024

Nomenclature

CCC	Considére & Continuity Criteria
CVGM	Cyclic Void Growth Model
DDS	Damage-Dominated Stage
DEC	Damage Evolution Criteria
FEA	Finite Element Analysis
FEM	Finite Element Method
GDDC	Generalized Ductile Damage Criteria
HHM	Hollomom Hardening Model
LHM	Linear Hardening Model
LPHM	Line-Power Hardening Model
PDS	Plasticity-Dominated Stage
RO	Ramberg-Osgood
RT	Rice-Tracey
SMCS	Stress Modified Critical Strain (Criterion)
VGM	Void Growth Model
VLCF	Very-Low Cycle Fatigue
WG	Working Group

Table of symbols

a_1, b_1	Material Constants for LHM
a_2, b_2	Material Constants for HHM
A_{VGM}	Constant Term (VGM)
CVN	Charpy Fracture Energy for a Sharp-V Notched Specimen
D_e	Damage Evolution Variable (DEC)
E	(Pristine) Material Young Modulus
E_{res}	Reloading Residual Material Stiffness (DEC)
F	Applied Force
f_y	Material Yield Strength
f_u	Material Ultimate Tensile Strength
G_f	Fracture Energy (DEC)
G_f*	Critical Fracture Energy (DEC)
J_1, J_2, J_3	Main (Deviatoric) Stress Tensor Invariants
k_s	Shear Sensitivity Parameter
L_{char}	Characteristic Length Parameter (DEC)
l^*	Characteristic Microstructural Size
P	Applied Load
R	Initial Radius of a Spherical Void (RT model)
R^2	Coefficient of Determination
R_0	Deformed Radius of a Spherical Void (RT model)
R*	Critical Radius of a Spherical Void (VGM)
S	Deviatoric Stress Tensor
s	Mesh size
t	Generic Time Step of a FEA
T	Stress Triaxiality Degree
t_i, t_f	Initial and Final Time Step of a FEA
u_{pl}	Plastic Displacement (DEC)
u_{pl}*	Critical Plastic Displacement (DEC)
VGI	Void Growth Index (VGM)
VGI_{cyc}	Cyclic Void Growth Index (CVGM)
VGI*	Critical Void Growth Index (VGM)
VGI^*_{cyc}	Critical Cyclic Void Growth Index (CVGM)
w	Relative Weight for LPHM
α	Toughness Coefficient (SMCS)
α_D	Material Parameter for Exponential DEC
α_{RO}, n_{RO}	Material Constants for RO Formulation
β	Triaxiality Exponent (VGM, SMCS)
Δ	Critical Strain Ratio [89]
ΔD	Diameter reduction
δ	Displacement
$\varepsilon_{0,Swift}$	Pre-strain Swift Constant
ε_{eng}	Engineering Strain
$\varepsilon_{eng,neck}$	Engineering Strain at Necking
$\boldsymbol{\varepsilon_{pl}}$	Plastic Strain Tensor
$\varepsilon_{pl,eq}$	Equivalent Plastic Strain (PEEQ)
$\bar{\varepsilon}_{pl,eq}$	PEEQ at a Generic Time Step in a FEA
$\varepsilon_{pl,eq,acc.}$	Accumulated PEEQ (CVGM)
$\varepsilon_{pl,eq,u}$	Ultimate PEEQ (DEC)
$\varepsilon_{pl,eq}$*	Critical PEEQ (SMCS)
$\varepsilon_{pl,eq,gen}$*	Generalized Critical PEEQ (GDDC)
$\varepsilon_{pl,ij}$	*ij*-th Component of the Plastic Strain Tensor
ε_{true}	True Strain
$\varepsilon_{true,neck}$	True Strain at Necking
$\varepsilon_{true,y}$	True Strain at Yielding
θ_s	Shear Stress Ratio
λ	Accumulated Plastic Strain Sensitivity Parameter (CVGM)
Φ	Ductility Reduction Ratio [89]
ξ	Lode Angle
Π	Plastic Displacement Ratio [89]
σ_{eng}	Engineering Stress
$\sigma_{eng,max}$	Maximum Engineering Stress
$\sigma_{eq,VM}$	Equivalent Von-Mises Stress
$\sigma_{eq,VM,D}$	Effective (Damaged) Von-Mises Stress (DEC)
σ_I, σ_{II}, σ_{III}	Principal Stresses
σ_m	Mean Pressure
σ_{true}	True Stress
$\sigma_{true,neck}$	True Stress at Necking
$\sigma_{true,y}$	True Stress at Yielding
Ω	Rivet Overstrength Ratio [89]
ω_D	Damage State Variable (GDDC)

specifically addressed the wide topic of design of steel structures assisted by FEM. Efforts from over ten years of work finally lead to the development of the new prEN1993–1-14:2023 [23] ("Design [of steel structures] assisted by finite element analysis"), which is currently in its enquiry phase before its final publication in 2025.

prEN1993–1-14:2023 gives principles and requirements for the use of numerical methods in the design of steel structures within the framework of a limit-state oriented design. Moreover, indications for advanced FEM modelling are also provided, i.e., specifying that its range of application is not confined to research purposes, but it also relates to design and safety assessment processes.

All the rules, which are expressly intended for designers who are experienced in the use of numerical modelling, are referred to two alternative approaches for FEM-based safety checks, i.e., (*i*) *analysis requiring subsequent design check*, according to which FEM modelling is used to reliably estimate the structural demand on components of interest, while safety verifications are carried out based on prescriptions reported in other parts of EN1993, and (*ii*) *direct resistance check*, according to which both the ultimate resistance of the structure and the relevant demand can be directly derived and compared. For both cases, different types of analyses with an increasing level of complexity are introduced (Fig. 1), i.e., starting from the simplest linear elastic analysis (LA) up to most refined geometrically and materially non-linear analysis with or without imperfections (GMINA or GMNA, respectively).

Notably, for direct resistance checks, which are recommended for the design and verification of crucial or complex structural assemblies, only analyses accounting for material non-linearity (MNA, GMNA, GMNIA) are allowed [23]. Therefore, a reliable and accurate material modelling is strictly needed, the validation of which shall be based on experimental evidences. Namely, according to prEN1993–1-14:2023, a validated numerical model has to correctly (or at least conservatively) capture each physical phenomena to be modelled. To this end is worth mentioning

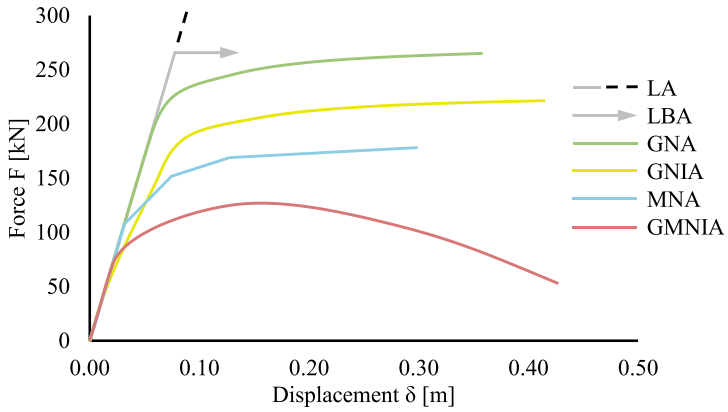

TYPE OF ANALYSIS	DEFORMATIONS	MATERIAL LAW	GEOMETRY
Linear elastic analysis (**LA**) Linear bifurcation (eigenvalue) analysis (**LBA**)	Linear Bifurcation	Linear elastic	Perfect
Materially non-linear analysis (**MNA**)	Non-linear	Elastic-plastic	
Geometrically non-linear analysis (**GNA**)		Linear elastic	
Geom. and mat. non-linear analysis (**GMNA**)		Non-linear	
Geom. non-linear analysis with imperfections (**GNIA**)		Linear elastic	Imperfect
Geom. and mat. non-linear analysis with imp. (**GMNIA**)		Non-linear	

Fig. 1. Allowed types of analysis according to prEN1993–1-14:2023.
(Adapted from [23]).

that, for typical cases, recommended material models are already given within the code.

Nevertheless, when assessing the ultimate resistance of components for which the governing failure mode is fracture (e.g., tension elements, bolts, plates with large plastic deformations), the use of cumulative damage models is prescribed, although no further hints about such models are reported [23], i.e., leaving the selection of consistent and reliable formulations to designers.

Therefore, the definition of some guidelines for the proper FEM-based prediction of fracture in steel structural components should be considered as an important task, i.e., not only for research purposes, but also to provide designers a comprehensive overview of available methodologies. The above considerations motivated the present work, in which a review of consolidated models to account for ductile damage and fracture in steel structural components is presented.

After recalling the most notable features of ductile fracture of metals, the following key topics are addressed in the following Sections: (*i*) post-necking constitutive behaviour of ductile steels, (*ii*) damage initiation criteria, (*iii*) damage evolution criteria up to failure and (*iv*) literature applications and/or extensions of such models for structural purposes. Each presented formulation is critically commented based on considerations reported by proposers and further researchers, i.e., based on a wide range of either seminal and more up-to-date works.

2. Generality about the ductile fracture of metallic materials

When at room temperature, ductile fracture is the typical failure mechanism for metallic materials [24,25]. Ductile fracture is a complex process that involves (*i*) large plastic deformations, (*ii*) progressive damage growth and (*iii*) subsequent fracture induced by coalescence of enlarged material voids, typically characterized by a significant reduction of the cross-section in a confined volume (necking) [26–29] (Fig. 2).

Loosely speaking, while before necking a significant degree of plasticity can be endured without a significant concentration of plastic strains, after necking a substantial localization and acceleration of material damage can be observed up to failure. Therefore, as widely acknowledged in scientific literature, two post-elastic behavioural stages can be identified for ductile metals before collapse, i.e., *plasticity-*

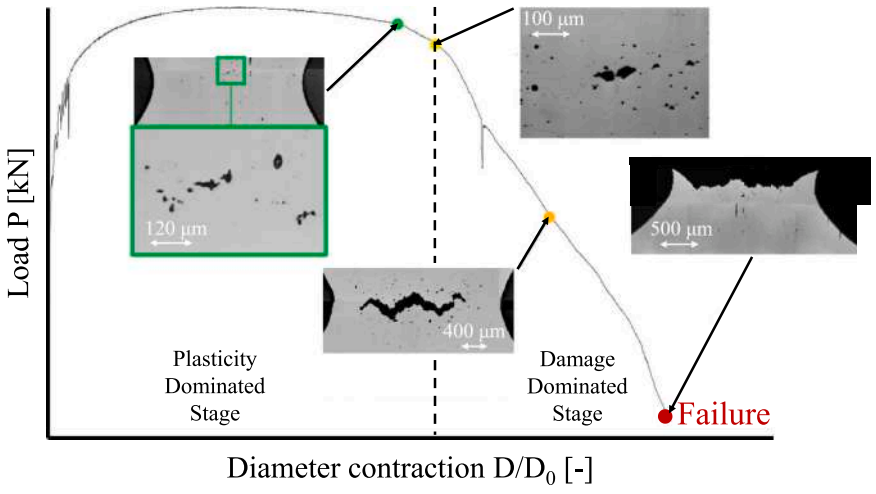

Fig. 2. Evolution of plasticity and damage in a round steel bar under uniaxial tension (Adapted from [27,28]).

dominated stage (hence also referred as "PDS") until the onset of necking and *damage-dominated stage* (hence also referred as "DDS") until fracture [30].

However, it is worth remarking that this distinction is somewhat conventional, as (*i*) on one hand, highly localized (i.e. at void scale) damage almost immediately occurs when the metallic component is experiencing PDS, while (*ii*) on the other hand, damaged material still behaves plastically, albeit showing degradation, up to void coalescence and fracture [31].

Nevertheless, for practical purposes in line with the scope of prEN1993–1-14:2023, PDS and DDS can be conveniently separated and addressed by means of distinct models, which can be hence individually calibrated and thus recoupled while analysing ductile fracture. This common approach is known as "uncoupled (damage) analysis" in scientific literature [32].

In the following Sections, after discussing the topic of post-necking behaviour of ductile materials, some of the main uncoupled damage models are introduced and critically reviewed.

3. Post-necking behaviour of ductile metals

While performing uncoupled analysis, it is necessary to define a post-necking plastic behaviour for the considered materials, i.e., due to "classic", constant-volume relations linking engineering and true stress-strain parameters being no longer valid after the onset of necking (Fig. 3). While performing an uniaxial tensile test, this condition can be easily recognized as the engineering stress-strain curve starts to decrease after reaching its maximum. In other words, necking manifests as an instability phenomenon occurring during tensile deformation, in which the specimen cross-section starts to decrease by a larger proportion than the material strain hardens [33].

As first recognized by Considére [34], necking onset can be hence identified by imposing that, immediately before diffuse necking, no net load increment dP (and thus, engineering stress $d\sigma_{eng}$) would occur for an infinitesimal increment of engineering strain $d\varepsilon_{eng}$ (*Considére criterion* [33,34] – Eqs. (1)–(2)):

$$d\sigma_{eng} = (d\sigma_{true} - \sigma_{true}\ d\varepsilon_{true})\exp(-\varepsilon_{true}) = 0 \tag{1}$$

$$d\sigma_{true} - \sigma_{true}\ d\varepsilon_{true} = 0 \rightarrow \frac{d\sigma_{true}}{d\varepsilon_{true}}\Big|_{necking} = \sigma_{true,neck} \tag{2}$$

A second, obvious condition at the onset of necking descends from the so-called *continuity criterion*, according to which the true stress at the onset of necking is the last stress value that can be estimated with constant-volume relations (Eq. (3)):

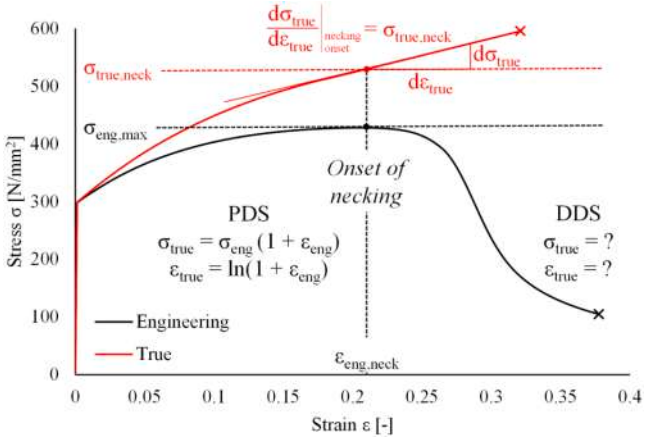

Fig. 3. Typical constitutive law of a ductile material in plasticity-dominated and damage-dominated stages up to failure (for the sake of simplicity, $\varepsilon_{eng,neck} \approx \varepsilon_{true,neck}$ is assumed).

$$\sigma_{true}|_{necking} = \sigma_{eng,max}\ (1+\varepsilon_{eng,neck}) = \sigma_{true,neck} \tag{3}$$

Thus, every analytical model attempting at capturing post-necking behaviour of a ductile material should fulfil conditions reported in Eqs. (1)-to-(3). It should be remarked that *Considére* and *continuity* criteria (hence also referred as "CCC") do not provide sufficient information about the shape of the post-necking branch of the true stress-strain curve, hence multiple formulations with increasing level of complexity can be adopted [33].

To this end, the simplest post-necking formulation is represented by the *linear hardening model* (hence also referred as "LHM"). Accordingly, the post-necking hardening branch of the true stress-strain curve can be modelled by means of a straight line (Eq. (4) and Fig. 4, black curve):

$$\text{LHM}: \sigma_{true} = a_1\ \varepsilon_{true} + b_1 \tag{4}$$

in which coefficients a_1, b_1 should be derived to ensure fulfilment of CCC (Eq. (5) – [33]):

$$\text{LHM}: \begin{cases} a_1 = \sigma_{true,neck} \\ b_1 = \sigma_{true,neck}(1-\varepsilon_{true,neck}) \end{cases} \tag{5}$$

It should be remarked that, although a_1 and b_1 are known when adopting LHM, the actual value of true strain at failure ($\varepsilon_{true,fail}$) is still unknown and should be calibrated according to tensile tests [33].

Another popular post-necking formulation is represented by the *power-law hardening model*, or *Hollomom hardening model* [35] (hence also referred as "HHM", see Fig. 4, red curve).

Accordingly, a power law expression can be used to capture the post-necking branch of the true stress-strain curve (Eq. (6)):

$$\text{HHM}: \sigma_{true} = a_2\ (\varepsilon_{true})^{b_2} \tag{6}$$

in which coefficients a_2, b_2 should be derived to ensure fulfilment of CCC (Eq. (7)), [33,35]:

$$\text{HHM}: \begin{cases} a_2 = \sigma_{true,neck}\ \left(\varepsilon_{true,neck}^{-\varepsilon_{true,neck}}\right) \\ b_2 = \varepsilon_{true,neck} \end{cases} \tag{7}$$

Similarly to LHM, HHM yields known a_2, b_2 constants, while the actual value of $\varepsilon_{true,fail}$ should be properly calibrated.

With respect to b_2 (also known as "*hardening exponent*" in scientific literature [36]), it is worth remarking that it is strictly included within the range {0.0; 1.0}, with 0.0 representing an ideal perfectly plastic material, while for $b_2 = 1.0$ the LHM is obtained once again.

It is worth reporting that, shortly after its introduction, HMM has been further refined by Swift [37], i.e., by introducing an offset term ($\varepsilon_{true} - \varepsilon_{0,Swift}$) in Eq. (7) in place of the lone total true strain. Although being slightly more complex (the pre-strain constant $\varepsilon_{0,Swift}$ should be

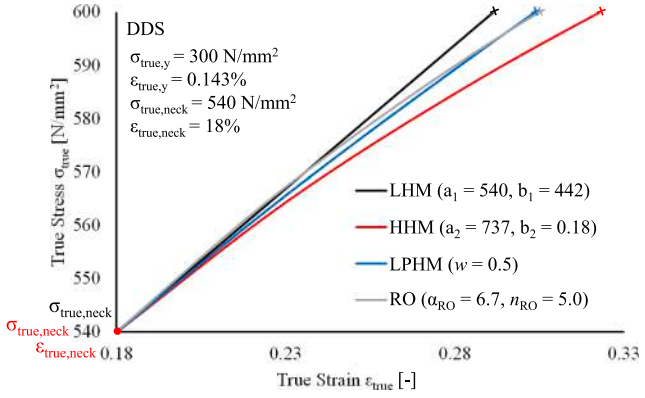

Fig. 4. Post-necking constitutive models for ductile metals: LHM (black curve), HHM (red curve), LPHM (blue curve), Ramberg-Osgood (grey curve).

calibrated based on tensile test results), Swift model can result in a more accurate post-necking modelling of some metallic alloys (e.g., Ti or Al alloys [38]).

"Hybrid" LHM-HHM formulations (*line-power hardening models* [39], hence also referred as "LPHM") can be also found in scientific literature, in which a weighted average between the two models is assumed by means of a relative weight w (Eq. (8) and Fig. 4, blue curve):

$$\text{LPHM}: \ \sigma_{true} = w\,(a_1 \ \ \varepsilon_{true} + b_1) + (1 - w)\,[a_2 \ \ (\varepsilon_{true})^{b_2}] \tag{8}$$

LPHM can, on principle, more accurately capture the post-necking behaviour of the considered material. However, a complex calibration procedure is required as both w and $\varepsilon_{true,fail}$ should be estimated based on experimental results [40]).

Although LHM, HHM and LPHM are among the most popular post-necking hardening models adopted in literature, it is worth noting that several more complex, yet reliable formulations are currently available, e.g. the saturation *Voce model* [41], three-parameters *Misiolek exponential hardening model* [42], or analytical *shape-depending* models, which attempt at deriving the triaxial post-necking stress field accounting for the shape of the tensile specimen (cylindrical, flat, etc. [33,41,42]).

The main drawback shared by all above formulations lies in their intrinsic piecewise nature. Indeed, each of the presented models only relates on the post-necking branch of the true stress-strain curve, hence a separate formulation should be used for the PDS up to the onset of necking (that is, constant-volume constitutive equations should be used). This issue can be overcome by adopting a continuous formulation which covers both PDS and DDS.

Among all the possible alternatives, the most popular formulation is arguably represented by the Ramberg-Osgood (RO) model [43] (Eq. (9) and Fig. 4, grey curve):

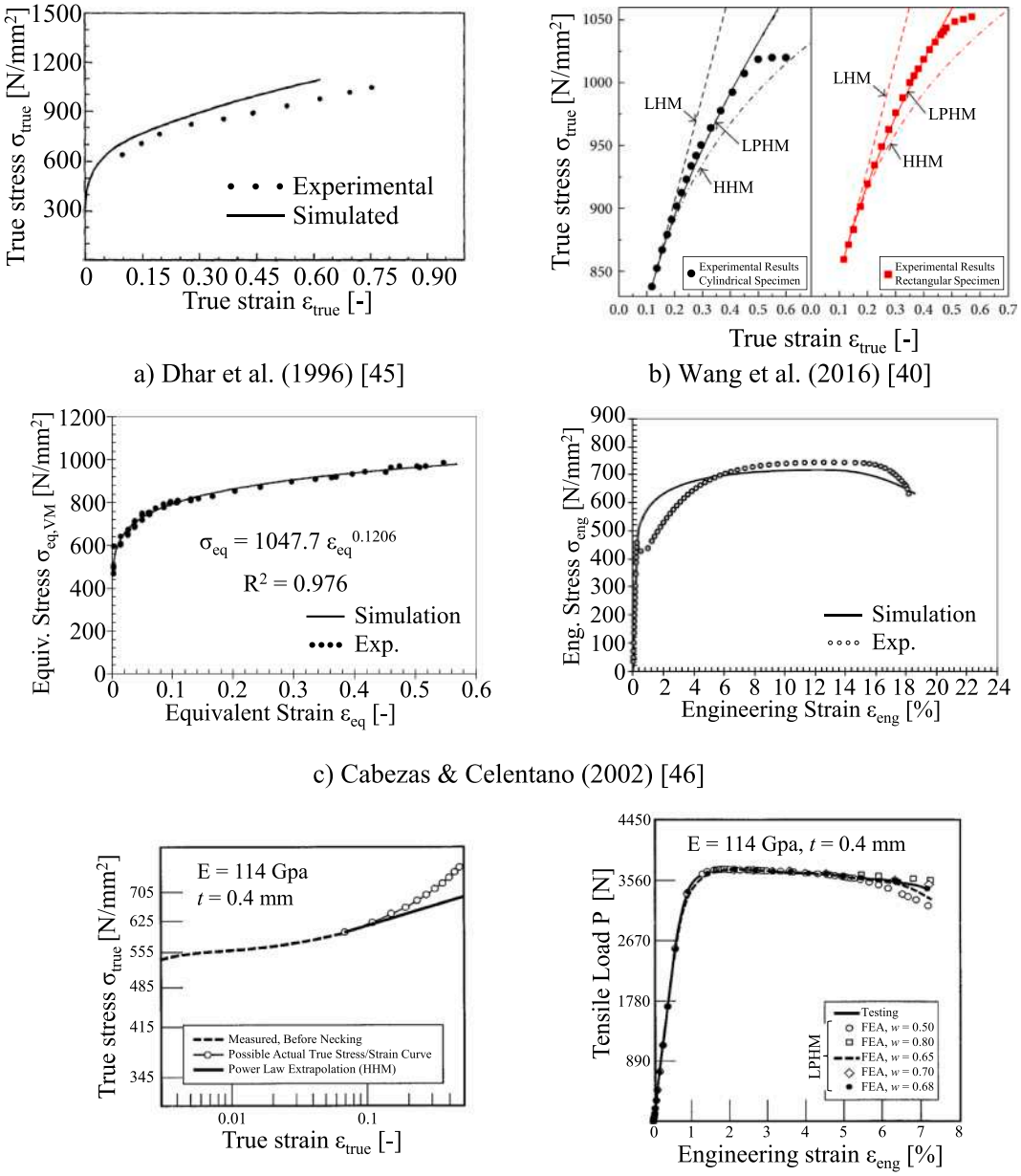

a) Dhar et al. (1996) [45]

b) Wang et al. (2016) [40]

c) Cabezas & Celentano (2002) [46]

d) Ling et al. (1996) [39]

Fig. 5. Examples of applications of post-necking constitutive models drawn from literature. (Adapted from [39,40,45,46]).

$$\frac{\varepsilon_{true}}{\varepsilon_{true,y}} = \frac{\sigma_{true}}{\sigma_{true,y}} + \alpha_{RO}\left(\frac{\sigma_{true}}{\sigma_{true,y}}\right)^{n_{RO}} \quad (9)$$

with $\varepsilon_{true,y}$ and $\sigma_{true,y}$ being the true strain and true stress at yielding, respectively, and α_{RO} (also known as "*yield offset*") and n_{RO} (also known as "*hardening exponent*") being empirical parameters which can be obtained by fitting experimental results.

It is worth remarking that, although able to capture true post-necking behaviour of materials, RO model is still most commonly used to fit engineering stress-strain data [36]. In this regard, it proves to be particularly useful when dealing with steels not having a clear yielding point, e.g., high strength steels, for which RO model is recommended by both EN1993–1-1 [44] and prEN1993–1-14:2023.

Nevertheless, when adopting true stress-strain RO formulation, a careful effort has to be placed in calibrating actual values of α_{RO}, n_{RO} and $\varepsilon_{true,fail}$ in order to obtain reliable results. Indeed, as the latter addendum in Eq. (9) is always non-null for $\sigma_{true} > 0$, plasticity is predicted to occur also in elastic range. The magnitude of this error, which represents the trade-off of adopting a continuous hardening model, can be controlled by appropriately manipulating yield offset and hardening exponent [36].

3.1. Strengths and limitations of reviewed post-necking formulations

Multiple attempts to use reviewed formulations to capture post-necking behaviour of steels can be found in scientific literature (Fig. 5 [39,40,45,46]).

On the basis of experiments performed by Le Roy et al. [47], Dhar et al. [45] adopted HMM to simulate the post-necking and damage behaviour of American SAE-AISI 1090 steel, i.e., a medium carbon steel (carbon content C_C = 0.85–0.98 %) with elevated yield and ultimate strength ($f_y \geq 540$ N/mm^2, $f_u \geq 700$ N/mm^2). According to Dhar et al., HMM is able to capture post-necking behaviour in uniaxial tension conditions, as a maximum error in terms of σ_{true} of about 8.0 % is achieved for a strain level of 55.0 % (Fig. 5a). Nevertheless, a slight lack of conservativity can be observed by comparing experimental and numerical results.

Interestingly, an opposite trend is reported by Cabezas & Celentano [46], which adopted HMM to simulate the post-necking behaviour of SAE-AISI 1045 thin-sheeted steel under uniaxial tension (Fig. 5c, C_C = 0.43–0.50, $f_y \geq 500$ N/mm^2, $f_u \geq 700$ N/mm^2). Indeed, while an exponential relationship successfully interpolates the material law in terms of equivalent stresses-strains (coefficient of determination $R^2 = 0.976$), the simulated engineering stress-strain curve is rather different with respect to experimental results.

Namely, while material strength for a given strain value is overestimated in PDS, the opposite condition occurs in DDS, where engineering stresses are underestimated up to failure ($\sigma_{eng,max} \approx 750$ N/mm^2 and 720 N/mm^2 according to experimental and numerical results, respectively, –5 %). This condition plausibly descends from (*i*) the approximation of constant-volume equations for a thin-sheeted specimen [33,42] and (*ii*) a certain level of conservativity related to HMM.

It is worth mentioning that analogous results were previously found by Ling et al. [39] with respect to other metals (Fig. 5d, C52100 phosphor bronze alloy), with the authors also claiming the lack of conservativity of LHM. This feature should be intended as intrinsic to the models themselves, as material parameters (a_1, b_1), (a_2, b_2) are fixed if CCC is deemed valid (see Section 3). This motivated the introduction of aforementioned LPHM, with one of the first examples of calibrations being indeed performed in [39].

A notable example of application of LPHM to structural steels is shown by Wang et al. [40], which further investigated the post-necking behaviour of SAE-AISI 1045 based on remarks reported by Cabezas & Celentano [46]. Accordingly, LPHM can very effectively predict the post-necking true stress-strain curve (Fig. 5b, solid lines) of both cylindrical and rectangular specimens, i.e., with comparable precision as respect to more complex models [33,41,42].

Nevertheless, it is worth remarking that quite different values of the relative weight w were obtained for such cases for the same nominal material ($w_{cyl.} = 0.153$ and $w_{rect.} = 0.234$, respectively). This implies a certain degree of conventionality in estimating material constants for LPHM, as shape-dependency cannot be fully eliminated. Moreover, as reported in [39,40], the estimation of relative weight can be quite difficult even for a single case, as repeated iterations are typically required. Nevertheless, based on reported outcomes, the following considerations can be drawn, i.e., (*i*) HMM is quite conservative and limited for steels at large values of strain, as already shown in literature; (*ii*) contrariwise, LHM is slightly unconservative, although very simple and closer to the actual material behaviour ($w < 0.5$ for both cases); (*iii*) LPHM can result in very accurate predictions, provided that w is reliably estimated based on experimental results; (*iv*) accuracy of a properly calibrated LPHM is comparable with other more complex post-necking models for steels.

4. Damage initiation criteria for ductile steels

4.1. Pioneering works related to damage of ductile metals

The next formulation required to perform uncoupled damage analysis of ductile metals is represented by a suitable damage model to capture material degradation in DDS. To this end, before addressing the topic of predictive damage models, it is worth recalling the phenomenology of ductile damage and fracture of metals.

Ductile fracture of metals occurs due to the nucleation and growth of microstructural voids, which are intrinsically present in metals as they surround inclusions and second-phase particles [48]. When subjected to multiaxial stress fields, such voids may get distorted and enlarged enough to cause local plastic deformations and necking (small-scale plasticity) up to *void coalescence*, which leads to macroscopical ductile fracture (Fig. 6).

In light of this peculiar phenomenology, it is clear that every attempt to analytically capture the nature of ductile fracture should account for void enlargement to some extent.

To this end, the pioneering contributions of McClintock [49] and Rice and Tracey [50] should be mentioned. In both works, ductile voids

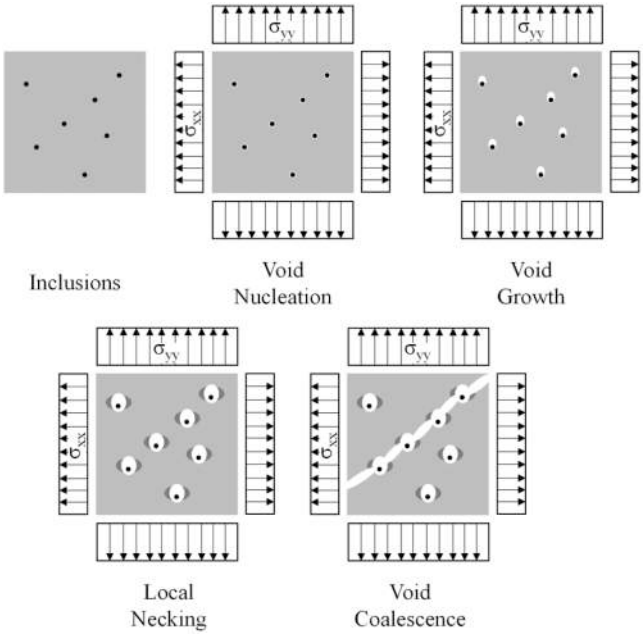

Fig. 6. Phenomenology of ductile fracture of metals. (Adapted from [48]).

enlargement in triaxial stress fields is addressed under some simplifying assumptions, namely:

(i) the base material is isotropic and obeys the Hencky-Von Mises ([51,52]) yield criterion;
(ii) the considered void is isolated;
(iii) an uniform stress field is remotely applied to the solid enclosing the void;
(iv) the undeformed void has an a-priori known geometry (cylindrical or spherical according to [49] or [50], respectively).

Based on the following assumptions, an analytical expression for the void size increase in dependence from applied remote stresses was derived. With reference to the lone Rice-Tracey (RT [50]) model, which met the highest popularity owing to a more realistic representation of voids, the following relation was derived (Eq. (10) [50]):

$$\ln\frac{R}{R_0} = \frac{3}{2}e^{-\frac{5}{3}\int_0^{\varepsilon_{pl,eq}} e^{\frac{3}{2}T}d\varepsilon_{pl,eq}} \tag{10}$$

with R being the deformed radius of the isolated void having initial radius equal to R_0, $\varepsilon_{pl,eq}$ being the equivalent plastic strain (PEEQ, Eq. (11)) and T being the so-called stress triaxiality degree (Eq. (12)):

$$\varepsilon_{pl,eq} = \sqrt{\frac{2}{3}\varepsilon_{pl,ij} : \varepsilon_{pl,ij}} \tag{11}$$

$$T = \frac{\sigma_m}{\sigma_{eq,VM}} \tag{12}$$

with $\varepsilon_{pl,ij}$ being the *ij*-th component of the plastic strain tensor $\boldsymbol{\varepsilon_{pl}}$ (":" denotes the scalar product operator), σ_m being the mean pressure, i.e., the arithmetic average of the three principal stresses $(\sigma_I + \sigma_{II} + \sigma_{III})/3$ and $\sigma_{eq,VM}$ being the equivalent Von-Mises stress.

It is worth remarking that, consistently with above formulations, PEEQ can be regarded as the direct "strain equivalent" of the Von Mises stress, while T allows to identify the nature of applied stress field (e.g., $T = 1/3$ for uniaxial tension or $T = 0$ for pure shear). Moreover, *sign*(T) allows to tell apart compressive ($T < 0$) from tensile ($T > 0$) stress fields, which result in shrinkage or enlargement of microstructural voids, respectively [53].

4.2. Void Growth Model (VGM)

Starting from the RT model, a damage initiation criterion based on void coalescence can be immediately formulated, i.e., by postulating the occurrence of damage for a critical value R^* of the deformed void radius (Eq. (13)–(14) [50,53,54]):

$$\ln R = \frac{3}{2}e^{-\frac{5}{3}}\ln R_0 \int_0^{\varepsilon_{pl,eq}} e^{\frac{3}{2}T}d\varepsilon_{pl,eq} = A_{VGM}\int_0^{\varepsilon_{pl,eq}} e^{\frac{3}{2}T}d\varepsilon_{pl,eq} = A_{VGM} \bullet VGI \tag{13}$$

$$R = R^* \rightarrow VGI = \int_0^{\varepsilon_{pl,eq}} e^{\frac{3}{2}T}d\varepsilon_{pl,eq} = VGI^* \rightarrow \text{Coalescence} \tag{14}$$

with A_{VGM} being a numerical coefficient recollecting all constant terms, VGI being the *Void Growth Index*, i.e., the integral on the right hand member which actually governs void growth and VGI* being the critical value of VGI for which damage is predicted.

The above model, known as Void Growth Model (VGM) in scientific literature, was first proposed by Rice and Tracey themselves as an extension of their void enlargement formulation [50,53]).

Critical Void Growth Index has to be intended as a material property, which should be calibrated on the basis of experimental results. According to [53,54], VGI* can be related to Charpy fracture energy for sharp-V notched specimens (CVN) as follows (Eq. (15)):

$$VGI^* \approx 0.018\ CVN - 1.30 \tag{15}$$

where CVN should be expressed in Joules in light of the empirical nature of the Equation.

In order to actually predict void coalescence, fulfilment of VGM criterion ($VGI \geq VGI^*$) has to be achieved in a finite neighbourhood of the plasticized zone having size l^* (characteristic microstructural size).

Actual values of l^*, which are intended as an intrinsic material constant, are usually within the range {10; 200} μm, and can be found in [53] for several steel alloys.

4.3. Stress Modified Critical Strain (SMCS) Criterion

In numerous realistic situations of monotonic loadings, the entity of stress triaxiality T remains substantially constant during the load history [53,55]. Therefore, as first noticed by Hancock & Mackenzie [56] this condition allows to directly calculate the critical equivalent plastic strain associated to coalescence $\varepsilon_{pl,eq}^*$ as a function of T, i.e., with higher triaxiality degrees leading to lower critical PEEQ and vice-versa.

This simplifying assumption underlies the so-called Stress Modified Critical Strain (SMCS) criterion [53,56], according to which $\varepsilon_{pl,eq}^*$ can be directly estimated as follows (Eqs. (16)-(17)):

$$VGI^* = \int_0^{\varepsilon^*_{pl,eq}} e^{\frac{3}{2}T}d\varepsilon_{pl,eq} \rightarrow \text{Coalescence} \tag{16}$$

$$\text{Coalescence}\,|_{T\approx const.} \rightarrow \varepsilon^*_{pl,eq} \approx \alpha\, e^{-\frac{3}{2}T} \tag{17}$$

with α being an empirical material parameter (usually known as "toughness coefficient") with a similar meaning to VGI* . According to [53], α can be related to CVN as follows (Eq. (18)):

$$\alpha \approx 0.016\ CVN - 0.93 \tag{18}$$

Similarly to Eq. (15), in the above expression CVN should be expressed in Joules in light of its empirical nature. In analogy with VGM, SMCS criterion predicts voids coalescence when $\varepsilon_{pl,eq} \geq \varepsilon_{pl,eq}^*$ in a finite region having size l^* .

The SMCS criterion is arguably simpler with respect to VGM, as it does not require the integration of triaxiality and equivalent plastic strain along the load path. Indeed, only an "instantaneous" check of PEEQ demand against $\varepsilon_{pl,eq}^*$ is needed, with the latter parameter being a function of the relevant stress triaxiality T.

Nevertheless, it should be remarked that, when T considerably changes during the loading history, the SMCS criterion may yield less accurate results with respect to the VGM [53].

4.4. Generalized ductile damage criteria

Both damage initiation criteria discussed earlier have the main drawback of requiring their fulfilment in a small, yet finite, neighbourhood of the plasticized zone having size equal to l^* (that is, few tens or hundreds of μm). Indeed, monitoring such a small volume can be really demanding, especially if this task is addressed as usual by means of finite element analyses (FEAs), as strongly refined meshes will be required [57,58].

To overcome this issue, characteristic volume-independent ("generalized") ductile damage criteria (GDDC) can be introduced by further extending RT void enlargement model. To this end, as suggested by Jia et al. [58], a damage state variable $\omega_D = \{0.0; 1.0\}$ can be introduced according to Eq. (19):

$$\omega_D = \int_{t_i}^{t_f} \frac{d\varepsilon_{pl,eq}(t)}{\varepsilon^*_{pl,eq,gen}(t;\ \sigma_{ij};\ \ldots)} \tag{19}$$

with t_i and t_f being the considered initial and final analysis steps, respectively and $\varepsilon_{pl,eq,gen}^*$ being a generalized critical equivalent plastic

strain, which can be, on principle, a function of the considered time step *t*, of the stress field (or appropriate combinations of stress variables) and, generally speaking, of other field variables such as temperature [59].

In light of a peculiar choice of $\varepsilon_{pl,eq,gen}^*$ trend, generalized ductile damage criteria can be "specialized" to model different materials. Nevertheless, when ω_D equals unity, punctual damage (i.e., generally speaking, *not* failure) is predicted to occur, and therefore the material locally starts to soften until macroscopic fracture.

The most immediate choice for $\varepsilon_{pl,eq,gen}^*$ is represented by the critical strain predicted by SCMS criterion (Eq. (17)). Although this choice leads to very similar results with respect to SMCS formulation, it should be remarked that, in this case, no assumptions are made on the control volume in which GDDC has to be fulfilled, as to each point is associated a distinct damage state variable.

It is worth remarking that, when selecting stress triaxiality T as the main parameter affecting the value of critical PEEQ, the use of an analytical expression to link these variables is not essential. Indeed, T-$\varepsilon_{pl,eq,gen}^*$ relation can be conveniently expressed via the so-called *triaxiality curves* [32,60]. Triaxiality curves can also directly account for the material strain rate dependence, if relevant [36].

The typical shape of triaxiality curves for ductile metals is depicted in Fig. 7.

As a corollary of findings reported in [50], triaxiality curves usually have a decreasing tendency for increasing values of T, with the worst condition represented by hydrostatic tension (T = 1).

However, as highlighted by Kõrgesaar [61] it is worth noting that metallic materials may have a non-monotonic T-$\varepsilon_{pl,eq,gen}^*$ trend when subjected to plane stress conditions, with a maximum value of critical equivalent plastic strain achieved for T ≈ 1/3. Indeed, when plane stress conditions are achieved (e.g., in case of in plane-loaded thin shells and plates), it can be observed a clear distinction between shear-failing specimens (T < 1/3) and necking-failing specimens (T ≥ 1/3). Nevertheless, generally speaking, the assumption of monotonically decreasing triaxiality curve can be considered sufficiently accurate for most practical purposes [32].

With regard to some metallic materials (e.g., Ti or Ni alloys [62]), a dependence of critical equivalent plastic strain on the so-called Lode angle $0 \le \xi \le \pi/3$ (Eq. (20) [63]) was also observed, i.e., the angle between the stress tensor projection on the deviatoric plane and the pure shear line [64]:

$$\xi = \frac{1}{3}\arccos\left(\frac{3\sqrt{3}}{2}\frac{J_3}{J_2^{3/2}}\right) \tag{20}$$

with J_2 and J_3 being the second and the third *main stress tensor invariant*, respectively (that is, stress invariants associated to the deviatoric stress tensor **S** [65]). In case of Lode angle-sensitive materials, *Lode curves* with analogous meaning to triaxiality curves can be conveniently defined

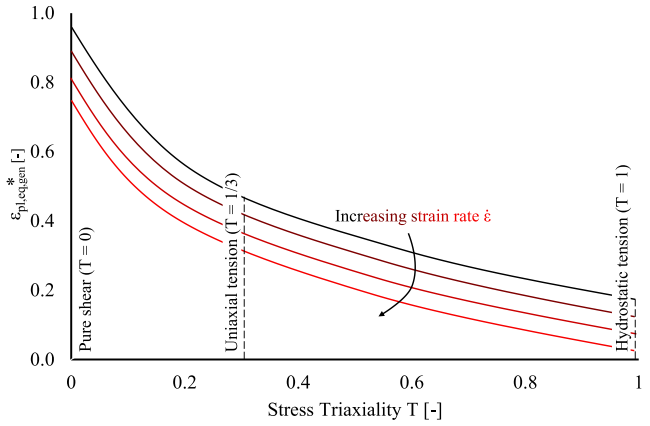

Fig. 7. Typical triaxiality curves for ductile metals.

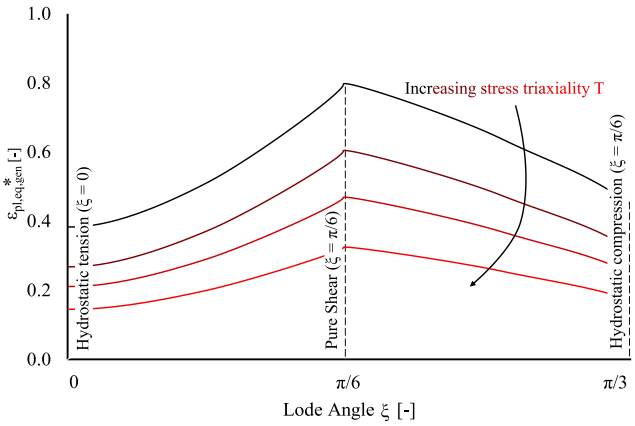

Fig. 8. Typical Lode curves for some ductile metals, e.g. Ti or Ni alloys. (Adapted from [66]).

(Fig. 8 – [66]) based on interpretation of coupled axial-torsional experimental tests [62,66].

Equivalently, shear fracture failure, when relevant, can be governed by means of the *shear stress ratio* $\theta_s = (k_s\,\sigma_m + \sigma_{eq,VM})/\tau_{max}$, with τ_{max} being the maximum shear stress and k_s being an experimental shear sensitivity parameter. Although few calibrated values of k_s can be found in literature with reference to ductile steel, it is worth reporting that a typical value of $k_s = 0.3$ is usually assumed for pure aluminium [67].

Finally, an explicit dependence on J_3 is also usually introduced in case of unsymmetric tensile-compressive fracture loci (e.g., in case of wrought and puddle iron, which show ductile compressive failure and brittle and premature tensile failure in light of the significant carbon content C > 2 % [68]).

Indeed, J_3 is the only main stress invariant parameter able to tell apart hydrostatic tension from hydrostatic compression, as J_2 is an even function and J_1 is identically null [65].

4.5. Hints on cyclic ductile fracture and cyclic void growth model (CVGM)

When assessing the ductile fracture of steel structural components in cyclic conditions, further complexities arise with respect to accurate damage modelling. Namely, mutations of the yield surface for repeated loading and unloading phases (cyclic hardening) should be properly accounted for [65].

Most common and simple formulations refer to either cyclic *isotropic hardening* (i.e., with the yield surface expanding with its centre being fixed) or cyclic *kinematic hardening* (i.e., with the centre of yield surface translating without any surface expansion). More complex and combined formulation are available in scientific literature, and are beyond the scope of this review. The interested reader may refer to [69–71] for a detailed theoretical framework and to retrieve calibrated parameters for common structural applications.

Nevertheless, with reference to GDDC, it is interesting to show some simple analytical advances developed by Kanvinde & Deierlein [57] to address cyclic damage of ductile metals, i.e., based on the theoretical background of the VGM (Cyclic Void Growth Model, hence also referred as "CVGM"). Namely, Kanvinde & Deierlein proposed a useful extension of ductile damage criteria with regard to cyclic loadings, that is, load histories in which T changes its sign multiple times.

Accordingly, fracture initiation is monitored by means of a cyclic Void Growth Index (VGI_{cyc}) which can be estimated according to Eq. (21) [57]:

$$VGI_{cyc} = \sum_{i-\text{th tensile cyc}} \int_{\varepsilon_{pl,eq,i}}^{\varepsilon_{pl,eq,i+1}} e^{\frac{3}{2}|T|} d\varepsilon_{pl,eq} - \sum_{j-\text{th compr. cyc}} \int_{\varepsilon_{pl,eq,j}}^{\varepsilon_{pl,eq,j+1}} e^{\frac{3}{2}|T|} d\varepsilon_{pl,eq} \tag{21}$$

Differently from monotonic VGM, (*i*) absolute value of stress triaxiality |T| is considered for calculations (that is, to correctly capture void shrinking for T < 0) and (*ii*) the integration over each *i*-th tensile and *j*-th compressive cycles is carried out separately, i.e., depending on the sign of the mean pressure σ_m.

According to [57], VGI_{cyc} should always remain non-negative. Therefore, when the index reaches zero (if it is the case) due to the contribution of a compressive cycle (in which the voids are shrinking, thus inhibiting coalescence), it stays null until the next tensile cycle [57].

Coalescence is predicted to occur when VGI_{cyc} reaches a critical value VGI^*_{cyc}, in a finite volume having characteristic size l^* . VGI^*_{cyc} can be expressed in function of fracture toughness parameter α (see Section 4.3) and accumulated PEEQ ($\varepsilon_{pl,eq,acc.}$) as follows (Eq. (22) [57]):

$$VGI^*_{cyc} = \alpha\, e^{-\lambda\, \varepsilon_{pl,eq,acc.}} \tag{22}$$

with λ being an experimental parameter which accounts for the material degradation under cyclic loads exceeding the elastic range. According to [57], recommended values for λ range between{0.4; 0.5} for most common structural mild steels.

VGI^*_{cyc} has to be updated at the end of each compressive cycle and stays fixed during the following tensile excursion (Fig. 9, red curve). In light of this, Eq. (22) further clarifies how α represents the asymptotic value of material fracture toughness for elements subjected to monotonic tensile stress histories (that is, in absence of cyclic degradation phenomena).

4.6. Strengths and limitations of reviewed ductile initiation criteria

Several examples of applications of reviewed damage initiation formulations for steels are available in scientific literature (Fig. 10 [32,58, 72,78–80]).

Tai [72] investigated the effectiveness of multiple damage initiation formulations [73–76] and proposed a new GDDC for steels (Fig. 10a). The Author noticed that all considered models, including the seminal RT formulation [50] converge for very low triaxialities (T → 0). Nevertheless, RT model proves to be highly conservative when assessing void growth at higher degrees of T. Tai ascribed such inconsistency to the assumption of rigid-perfectly plastic material introduced by Rice & Tracey [50]. Notably, a far better match between prediction and experimental results drawn from Brownrigg et al. [77] (SAE-AISI 1045 steel) is achieved if strain hardening is more precisely accounted for, e.g., by means of a RO formulation [43].

Tai also showed how triaxiality curves actually change for different values of the hardening exponent n_{RO}, with Rice & Tracey model becoming an asymptotic condition for n_{RO}→ 0. Therefore, RT model, although still widely used in light of its intrinsic simplicity, should be limited to moderate triaxialities and moderate strain hardening capabilities.

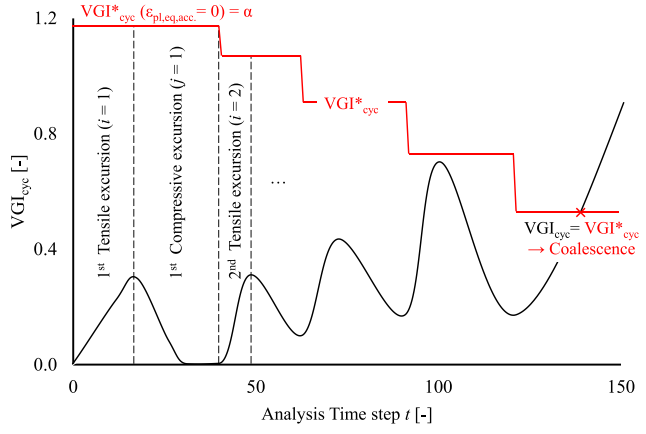

Fig. 9. Graphical interpretation of predicted coalescence in CVGM. (Adapted from [57]).

Kiran & Khandelwal addressed the ductile fracture of cylindrical notched specimens made of ASTM A992 steel, i.e., a mild steel commonly adopted for American wide-flange I-shaped profiles (Fig. 10b [78], C_C = 0.25–0.29 %, $f_y \geq 345$ N/mm^2, $f_u \geq 450$ N/mm^2). For instance, Kiran & Khandelwal attempted to simulate the monotonic response of both blunt- and sharply notched coupons accounting for high stress triaxiality arising at the notch tip (T = 0.5–1.0 [78]).

For this purpose, both VGM and SMCS criteria were used and properly calibrated. According to [78], high values of T significantly reduce ASTM A992 ultimate ductility, with the location of ductile fracture being well correlated with the spot showing the peak triaxiality level.

Nevertheless, as noticeable from simulation results (Fig. 10b, solid black curves), VGM and SMCS criteria both overestimate the stress state in DDS for all specimens up to failure. This clearly descends from the absence of a damage evolution formulation, which should be coupled to aforementioned models to more precisely capture failure. Still, specimens ductility can be properly simulated through accurate calibration. Kiran & Khandelwal also claimed that: (*i*) in line with remarks from Tai [72], the triaxiality exponent β = 3/2 suggested by Rice & Tracey [50] may be inadequate for ductile steels due to strain hardening, while a material-depending value could be used (β = 1.15 is suggested for A992 steel); (*ii*) SMCS model, although being much simpler than VGM, results in different values of α depending on the specimen shape (that is, α = 2.62 or 5.00 for sharp-notched and blunt-notched cylinders, respectively), i.e., with such inconsistency being a consequence of neglecting the variable stress history at notches' tip; (*iii*) contrariwise, VGM model is able to capture the ductile failure of all specimens through a single calibrated value of VGI* (=3.482 for A992 steel, provided that β = 1.15 is assumed), although with a stronger computational effort.

With reference to GDDC, it is worth mentioning contributions published by Jia et al. [58] and Yang & Veljkovic [32]. On one hand, the former researchers simulated the monotonic ductile fracture of Japanese SS400 (C_C = 0.17 %, f_y = 270 N/mm^2, $f_u \geq$ 460 N/mm^2), HT800 (C_C = 0.20 %, f_y = 763 N/mm^2, f_u = 826 N/mm^2) and SM490 (C_C = 0.13 %, f_y = 401 N/mm^2, f_u = 546 N/mm^2) steels based on experiments performed by Kuwamura & Yamamoto [81] and Arita & Iyama [82] (Fig. 10c).

Damage initiation was predicted according to the expression reported in Eq. (19), i.e., coupled with SMCS model for the estimation of $\varepsilon_{pl,eq}{}^*$. A good agreement between experimental and numerical curves can be observed for each investigated material, although simulated damage onset always exceeds experimental values by some amount (+4–90 % in terms of diameter reduction ΔD at crack initiation, mean error +32 %, see Fig. 10c, black and white triangles). Moreover, Jia et al. pointed out that only a slight mesh dependency was observed. However, this may depend on the simplicity of simulated geometries.

On the other hand, Yang & Veljkovic calibrated plasticity and damage models for two European structural steels, i.e., S275 mild steel (C_C = 0.19–0.23 %, $f_y \geq$ 275 N/mm^2, $f_u \geq$ 430 N/mm^2) and S690 high strength steel (C_C = 0.19–0.23 %, $f_y \geq$ 690 N/mm^2, $f_u \geq$ 770 N/mm^2). Yang & Veljkovic proposed an easily calibratable expression to define triaxiality curves for steels based on RT model (Fig. 10d). Accordingly, the entire T-curve can be defined based on the critical PEEQ for uniaxial tension $\varepsilon_{pl,eq}{}^*$ (T = 1/3), with such parameter being simply derivable from coupon tests. This approach can be particularly useful for practical purposes, and it retains the physical behaviour of steels under variable levels of stress triaxiality. Nevertheless, it should be remarked that: (*i*) a significant mesh sensitivity is expected, hence preliminary sensitivity analyses are required [32]; (*ii*) the approach may show limited effectiveness in case of significant strain hardening (as it underlies a fixed value of β = 1.5 [72,78]) and/or for thin-sheeted or shear-dominated components (as monotonicity of triaxiality curves would not be granted [61]).

With reference to cyclic ductile fracture, although only basic insights

are given in the present review, it is still interesting to show few recent examples of application of the CVGM that can be retrieved in literature (Fig. 11 [79,80]).

Tartaglia et al. [79] adopted CVGM to predict cyclic failure of complex structural assemblies (in very-low cycle fatigue (VLCF) conditions. Namely, Tartaglia et al. computationally implemented CVGM to assess cyclic weld rupture in a non-code conforming steel joint belonging to an existing multi-storey steel structure (i.e., conservatively assuming the occurrence of macroscopic weld fracture immediately after void coalescence – Fig. 11a). Predicted values of joints' rotational capacity (i.e., governed by fillet welds) comply with the typical performance of pre-Northridge, non-seismically designed American steel connections [79,83].

Nevertheless, it is worth remarking that, as reported in [79], the application of CVGM proved to be strongly mesh size-dependant (a minimum mesh size $s = 1$ mm was finally adopted to balance analyses accuracy and computational effort) and time-consuming. Therefore, preliminary sensitivity analyses are recommended when assessing the cyclic fracture of full scale structural assemblies.

Analogous considerations were pointed out by Moradnezhad et al. [80], which employed CVGM to predict the ductile failure of innovative knee-brace devices for the seismic retrofitting of existing

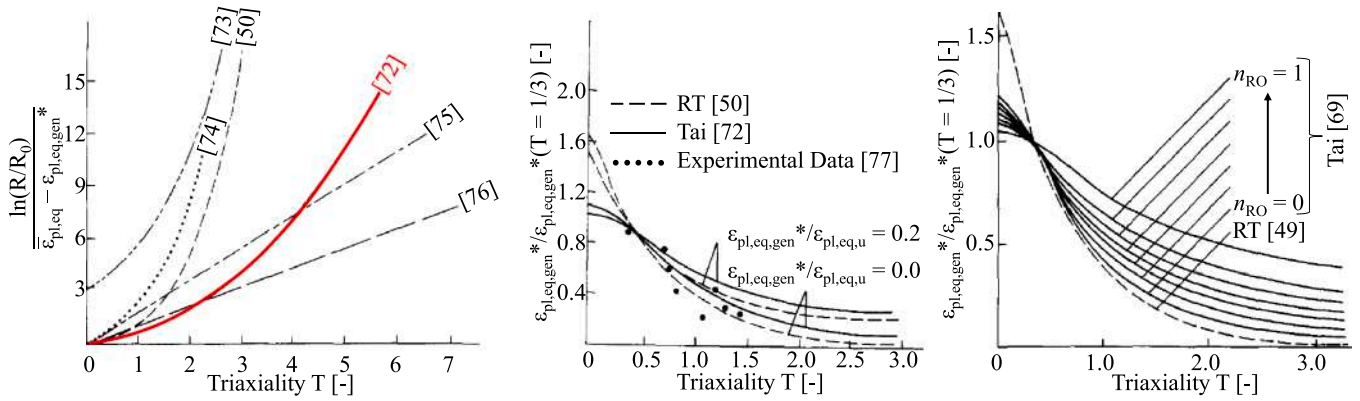

a) Tai (1990) [72]

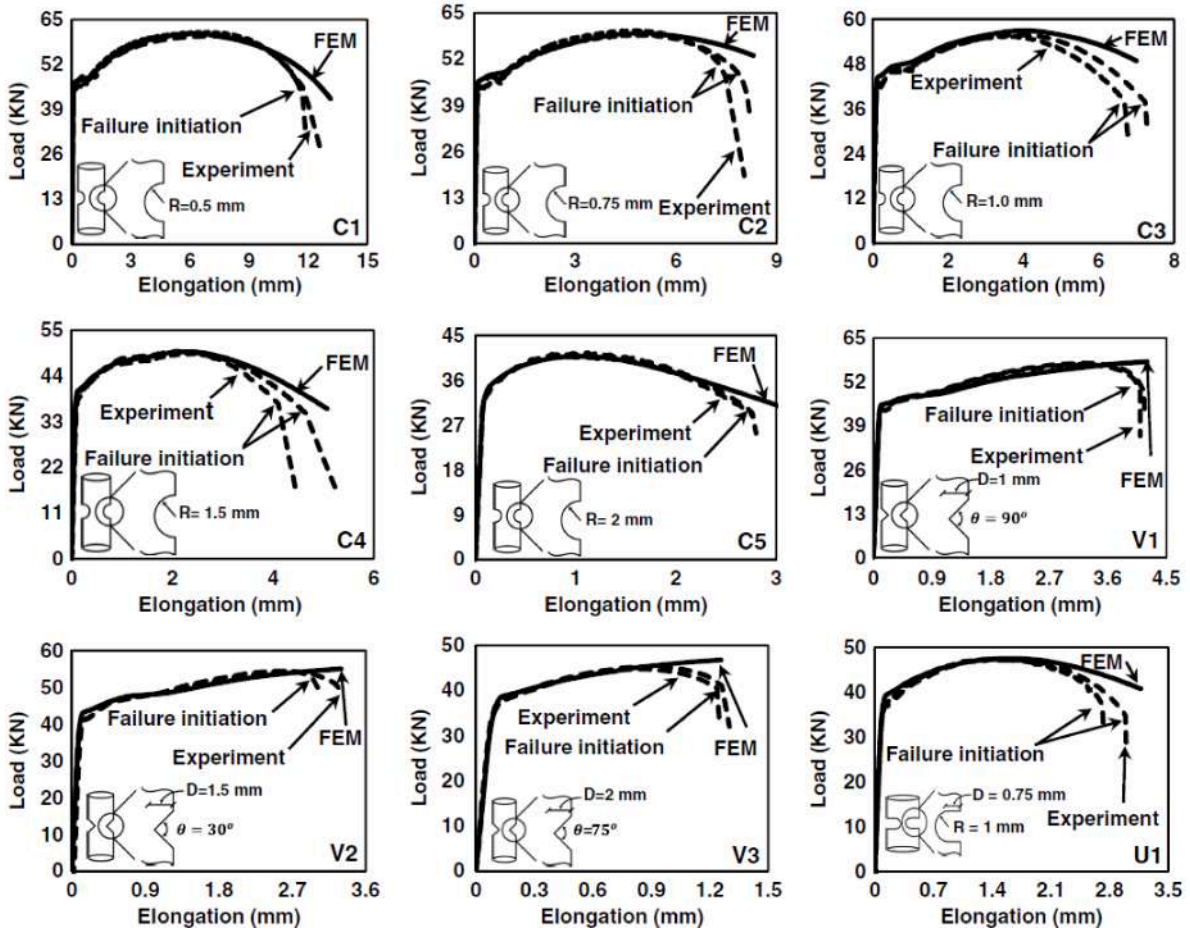

b) Kiran & Khandelwal (2014) [78]

Fig. 10. Examples of applications of monotonic damage initiation models drawn from literature. (Adapted from [32,58,72,78]).

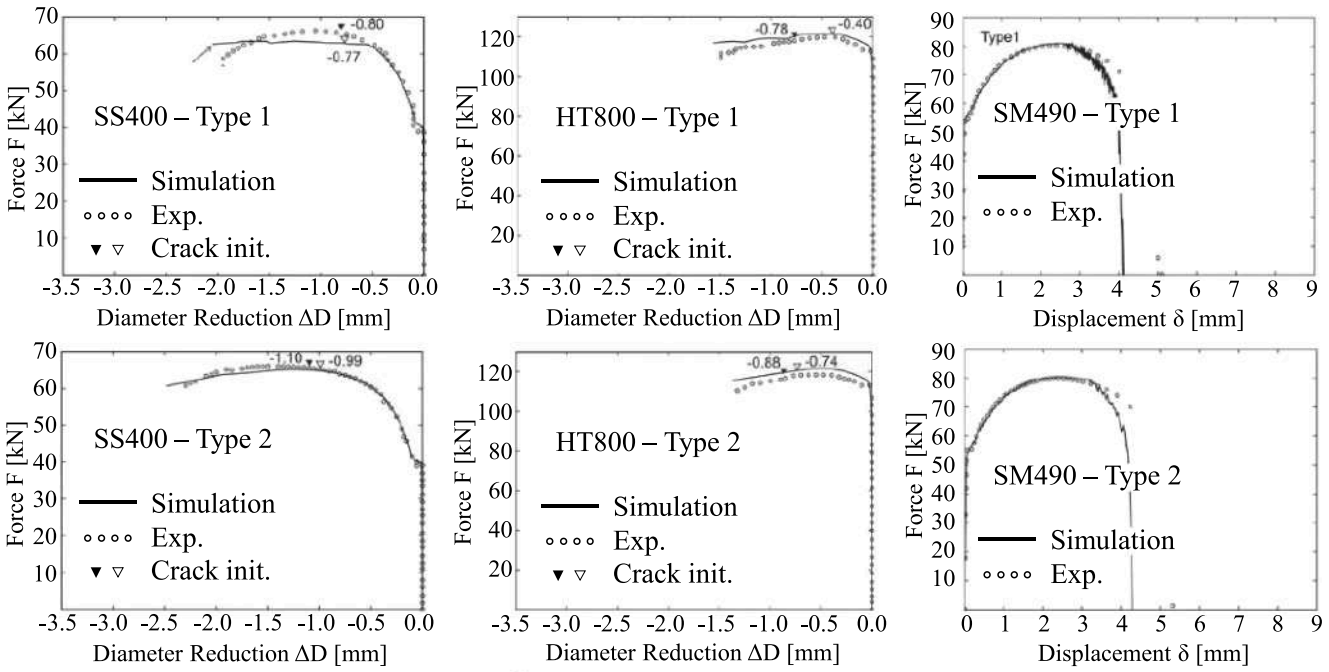

c) Jia et al. (2014) [58]

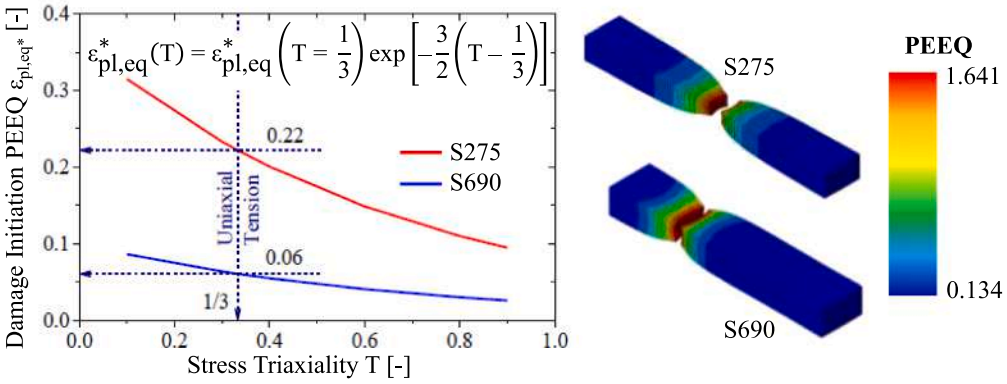

d) Yang & Veljkovic (2019) [32]

Fig. 10. (*continued*).

moment-resisting steel frames. Accordingly, hysteretic behaviour of such components under cyclic tensile and compressive forces can be accurately predicted not only in terms of ultimate resistance and ductility, but also with respect to deformed configuration at failure (Fig. 11b). Nevertheless, a rather fine mesh was required in spite of the simplicity of investigated components.

5. Damage evolution criteria

As anticipated in Section 4.4, when GDDC are adopted to capture ductile failure of metals, proper *damage evolution criteria* (DEC) could be also introduced to account for material damaged behaviour for $\varepsilon_{pl,eq} \geq \varepsilon_{pl,eq,gen}^{*}$. Indeed, as opposed to VGM, SMCS and CVGM criteria, GDDC may account for a residual, post-cracked stiffness of materials before macroscopic fracture [58].

As first postulated by Hillerborg et al. [84] with reference to cementitious concrete, a single damage evolution variable $D_e = \{0.0; 1.0\}$ can be introduced to manipulate the equivalent (Von-Mises) stress-strain constitutive law up to failure (that is, to capture post-cracking softening – Eq. (23)):

$$\sigma_{eq,VM,D} = (1 - D_e) \quad \sigma_{eq,VM} \tag{23}$$

with $\sigma_{eq,VM,D}$ being the "effective" Von-Mises equivalent stress for the damaged material.

Consistently, extreme values of $D_e = 0.0$ and $D_e = 1.0$ are associated to a pristine and a completely failed material, respectively. Notably, Hillerborg formulation proved to be also valid for ductile steels in DDS, and it is now included in most software for refined structural analyses [9,10].

It is worth remarking that, in the most general case of non-monotonic loadings, D_e both affects (*i*) the material "effective" yield stress and (*ii*) the re-loading residual stiffness $E_{res} = (1 - D_e)\ E$, with E being the pristine material Young Modulus (Fig. 12 [84]).

Among the several literature proposals, two approaches linking the damage evolution variable with equivalent plastic strains gained the highest popularity, i.e. the *energy-based approach* and the *displacements-based approach* [84–87].

Accordingly, D_e monotonically increases depending either on the dissipated fracture energy G_f (Eq. (24)) or on the plastic displacement u_{pl} (Eq. (25)) up to failure, respectively:

$$G_f = \int_{\varepsilon^{*}_{pl,eq,gen}}^{\bar{\varepsilon}_{pl,eq}} L_{char} \quad \sigma_{eq,VM,D} \quad d\varepsilon_{pl,eq} \tag{24}$$

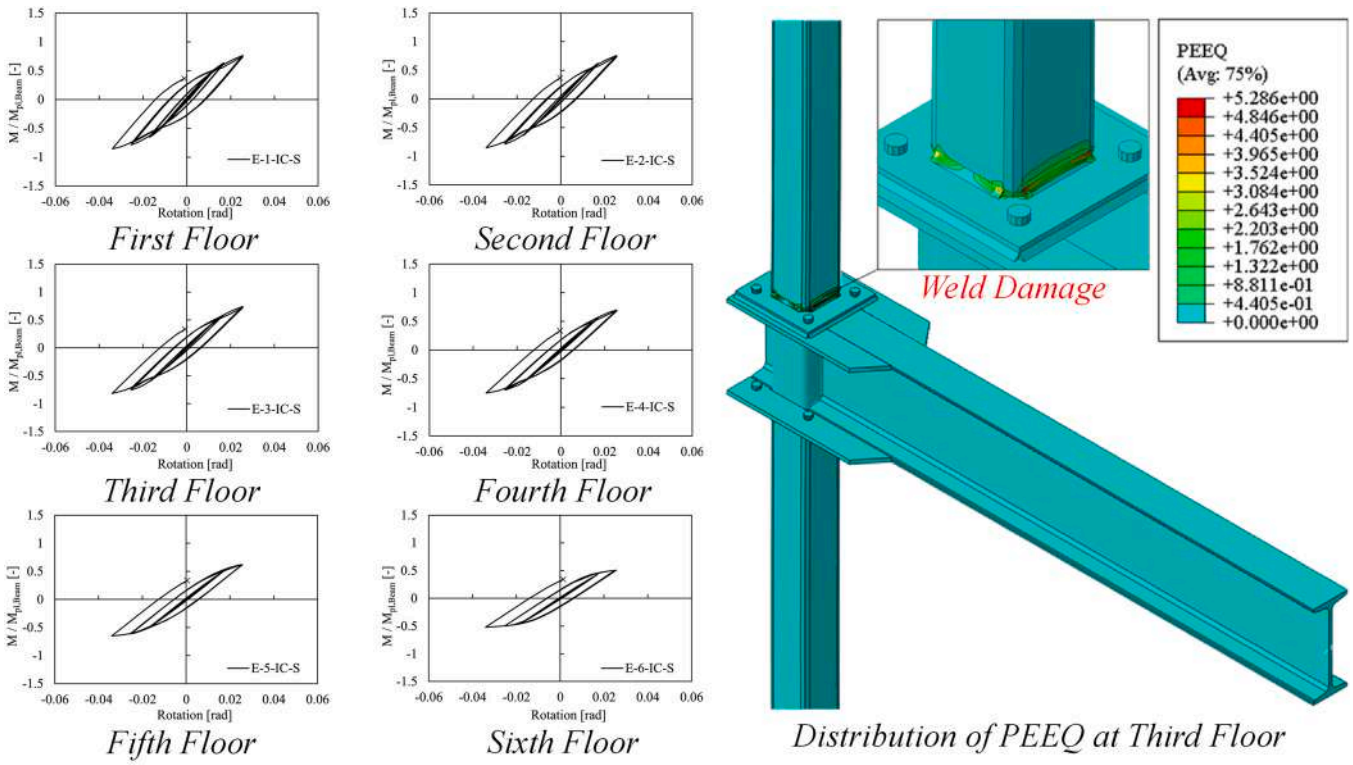

a) Tartaglia et al. (2022) [79]

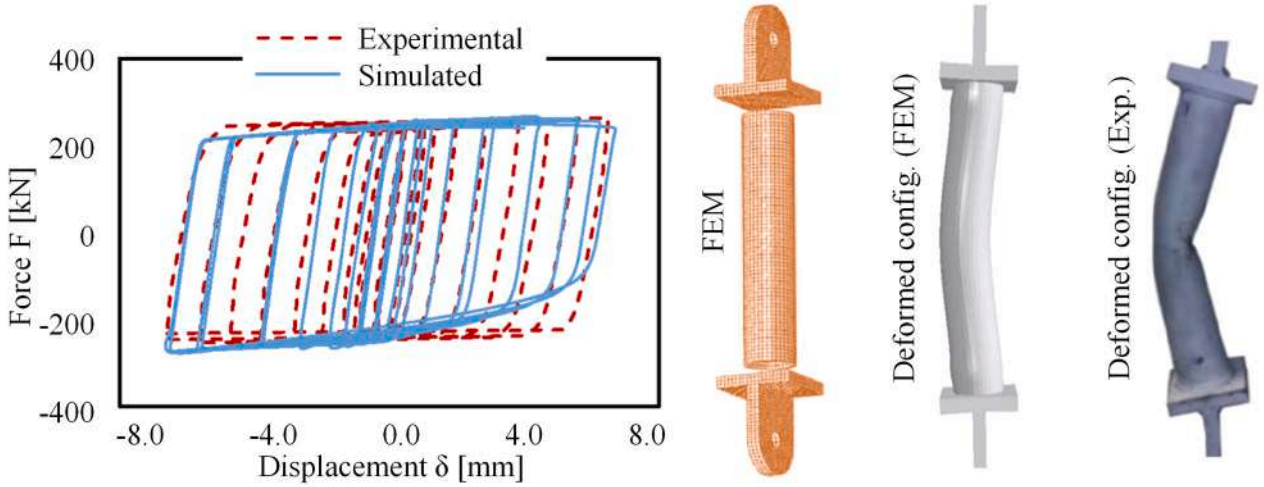

b) Moradnezhad et al. (2023) [80]

Fig. 11. Examples of applications of CVGM drawn from literature. (Adapted from [79,80]).

$$u_{pl} = L_{char}\left(\bar{\varepsilon}_{pl,eq} - \varepsilon^{*}_{pl,eq,gen}\right) \quad (25)$$

with $\bar{\varepsilon}_{pl,eq}$ being the PEEQ ($\geq \varepsilon_{pl,eq,gen}^{*}$) for a given analysis step and L_{char} being a characteristic length parameter.

Notably, the introduction of L_{char} in both G_f and u_{pl} definitions is not coincidental, as both quantities were conceived to be implemented in the framework of the Finite Element Method. Namely, by including a characteristic length in damage evolution monitoring, the strong mesh dependency exhibited by dissipated energy, yield stress and plastic strains for a damaged material can be effectively mitigated [84–87].

In both cases, critical values of G_f^{*} and u_{pl}^{*} are assumed to be attained in correspondence of a (conventional) ultimate equivalent plastic strain $\varepsilon_{pl,eq,u}$ (that is, failure is predicted to occur when $\bar{\varepsilon}_{pl,eq} = \varepsilon_{pl,eq,u}$ in Eqs. (24)-(25)). Conventionality of $\varepsilon_{pl,eq,u}$ derives from the impracticability, in many real situations, of its explicit derivation on the basis of experimental outcomes. For practical purposes, the direct estimation of G_f^{*}or u_{pl}^{*} is usually pursued with the aid of numerical tools to interpretate test results [32].

Although the energy-based formulation is sometimes used when dealing with some Ti, Cu or Ni alloys [86], it is worth noting that the displacement-based approach proves to be the most suitable one for ductile metals. To this end, both linear (Eq. (26)) and exponential (Eq. (27)) trends have been proposed to describe the functional link among u_{pl} and D_e [87]:

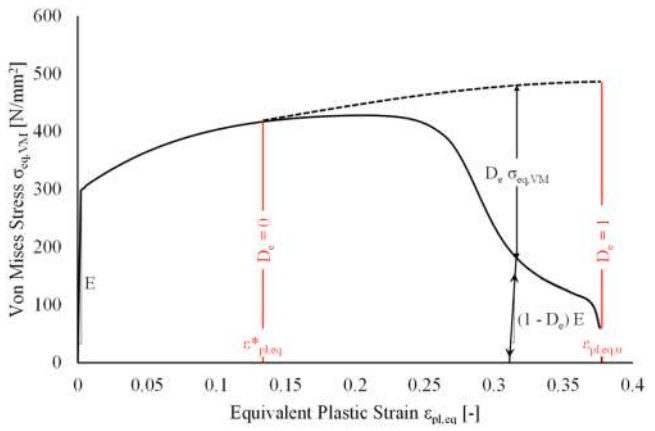

Fig. 12. Typical softening behaviour of a damaged material according to DEC. (Adapted from [84]).

$$\text{Linear DEC}: \ D_e = \frac{u_{pl}}{u^*_{pl}} \tag{26}$$

$$\text{Exponential DEC}: \ D_e = \frac{1 - e^{\alpha_D \left(u_{pl} / u^*_{pl} \right)}}{1 - e^{\alpha_D}} \tag{27}$$

with $\alpha_D \geq 0$ being an experimental parameter accounting for damage-displacement non-linearity.

Notably, linear DEC can be considered as a degenerate case of exponential DEC for $\alpha_D \rightarrow 0$ (Fig. 13). Moreover, when such analytical relations are used to link the damage state variable and the plastic displacement, equivalent energy-based formulations can be immediately deduced by observing that G_f is directly proportional to the underlying area in the $\sigma_{eq,VM}$ - u_{pl} plane for any given value of u_{pl}. For example, regarding to the simplest case of linear DEC, it can be easily derived that $G_f = u_{pl}\ \sigma_{eq,VM}/2$ [87].

5.1. Strengths and limitations of reviewed damage evolution criteria

As pointed out in the previous Section, DEC are almost always adopted in combination with damage initiation formulations [85–87]. Therefore, literature works concerning the lone damage evolution phase in ductile steels are quite hard to find. Nevertheless, some key remarks about strengths and limitations of reviewed DEC can still be drawn based on aforementioned contributions from Tai [72] and Dhar et al. [45] (Fig. 14).

For instance, within the framework of its extended damage model for

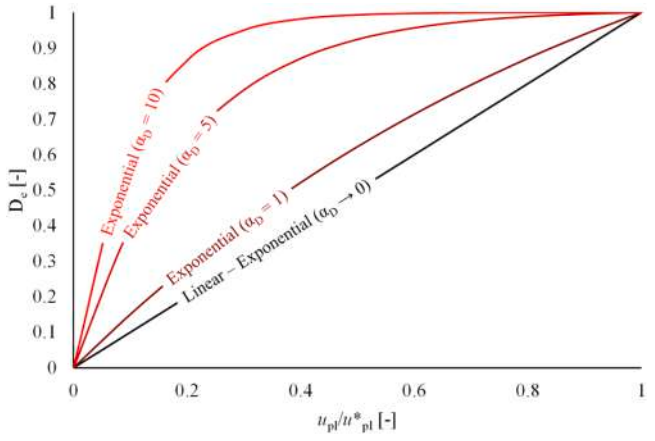

Fig. 13. Graphical representation of linear and exponential displacement-based DEC.

SAE-AISI 1045 steel, Tai observed three stages while monitoring damage state variable D_e, i.e. (*i*) damage generation (Stage I), in which damage is very small principally ascribed to void nucleation; (*ii*) damage (stable) growth (Stage II), in which D_e is related to void growth; (*iii*) damage (unstable) acceleration (Stage III), in which void coalescence occurs, and hence damage varies suddenly (Fig. 14a [72]). Most notably, damage evolution in Stage II is almost linear with respect to plastic strains, i.e., complying with assumptions of the most simple linear DEC, with simulated damage matching well the experimental points [77]. On the other hand, Dhar et al. [45] proved that the critical damage value, which can be interpreted as proportional to u_{pl}^* up to a scale factor, is almost independent on both the specimen shape and triaxiality at failure (Fig. 14b [45]). This implies that adopting two independent, yet linked formulations for damage initiation and damage evolution is a consistent choice, as u_{pl}^* can be regarded as an intrinsic material parameter to be calibrated on a case-by-case basis.

6. Comprehensive applications of reviewed models for structural purposes

In this final Section, some comprehensive literature applications of reviewed damage models are presented as respect to refined assessment of steel structural components (Figs. 15–17 [88–90]).

Yang et al. [88] simulated the tensile fracture of fully and partially threaded high-strength bolts based on experimental tests performed by Grimsmo et al. [91] (Class 8.8, $f_y \geq 640$ N/mm2, $f_u \geq 800$ N/mm^2 – Fig. 15). For this purpose, Yang et al. introduced (*i*) a LPHM to capture post-necking behaviour of high-strength steel (constant-volume equations were used for pre-necking stage), (*ii*) non-monotonic triaxiality curves according to the two-parameter formulation proposed by Bao & Wierzbicki [92] and (*iii*) linear DEC with element deletion and very small u_{pl}^* value (= 0.001 mm).

Each component of bolt assemblies (threaded screws, nuts, washers) was discretized through solid C3D10M elements (tetrahedrons, quadratic geometry, modified formulation). Namely, a rather fine mesh (variable size, $s = 0.5$–1.5 mm) was adopted based on preliminary sensitivity analyses.

Interestingly, Yang et al. manipulated LPHM beyond intended values of relative weight w, as negative values of w (up to –0.4) were also considered to model post-necking stage. As a result, true stress-strain constitutive behaviour of high-strength steel softens after necking (the larger the absolute value of $|w|$, the stronger the softening). It is worth highlighting that such an assumption does not comply with the actual material behaviour, as undamaged true stress in steels always increase up to failure [33,36]. Nevertheless, adopting a negative w value may improve analysis convergence, as an aliquot of ductile damage evolution is equivalently incorporated in the base material constitutive law. Besides, this inconsistency may be considered less relevant for high-strength steels, as their post-necking stage is typically shorter as respect to mild steels owing to reduced ductility [93,94].

With reference to DDS, it is worth reporting that (*i*) differently from works based on RT model [50], void-formation dominated range ($T > 1/3$) is modelled through an hyperbolic function based on tensile tests on stocky cylindrical specimens [88,92] and (*ii*) a very short damage evolution phase was considered, i.e., in compliance with higher brittleness of high-strength steels [93,94].

In light of the accurate calibration, tensile fracture of both fully threaded (FT118) and partially threaded (PT130) bolts is very effectively captured, that is, both in terms of force-displacement curves up to failure and PEEQ distributions in fractured configurations.

With respect to more complex structural assemblies, it is worth to first mention the recent work of Milone et al. [89], which addressed the influence of constructional imperfections on the static performance of lap-shear hot-driven riveted connections, which are commonly found in existing railway steel bridges in service [95,96]. In order to parametrically investigate the impact of such imperfections, Milone et al.

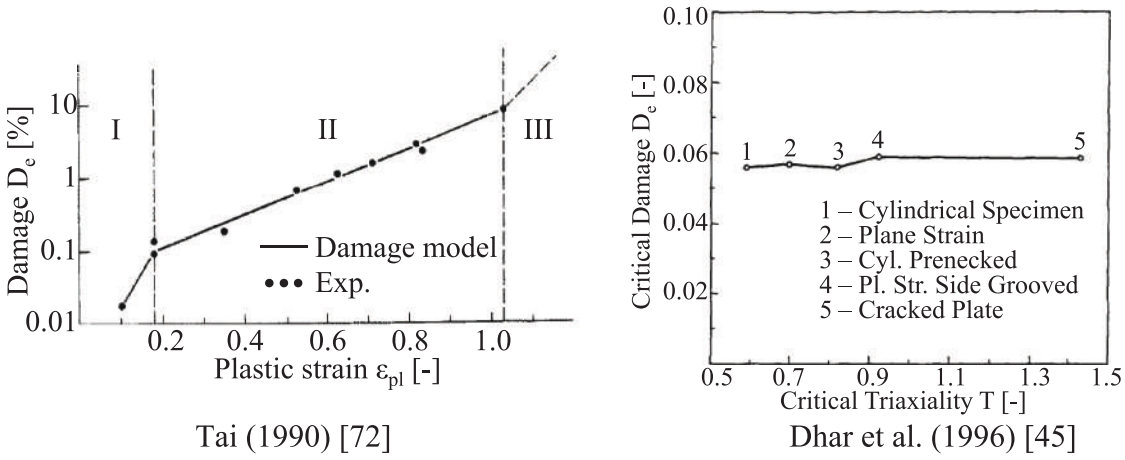

Fig. 14. Examples of applications of damage evolution models drawn from literature. (Adapted from [45,72]).

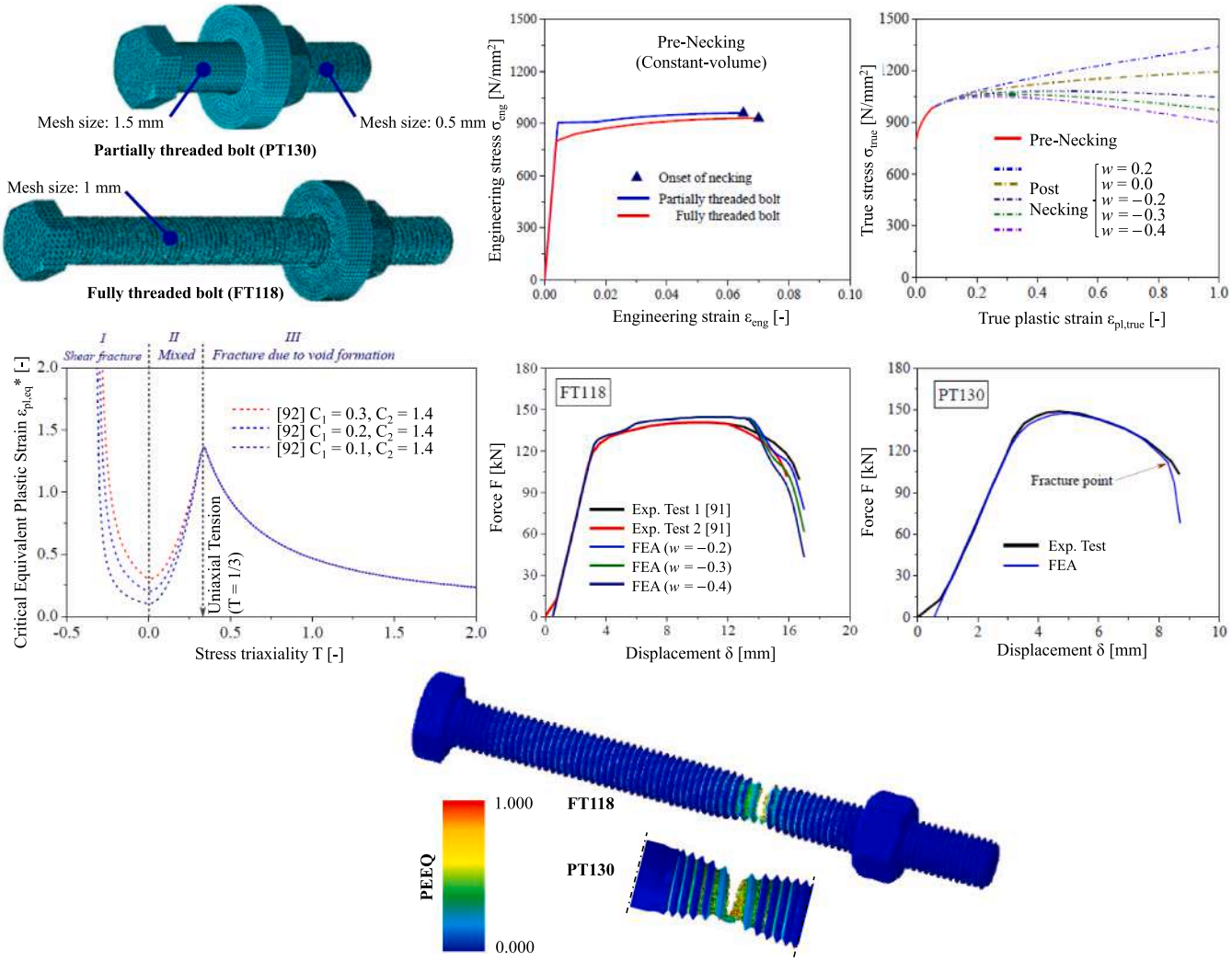

Fig. 15. Examples of application of reviewed damage models for structural purposes: tensile fracture of partially and fully threaded bolts. (Adapted from [88]).

first calibrated refined finite element models on pristine connections based on experimental tests performed by D'Aniello et al. [97]. Accordingly, the following modelling assumptions were considered to model ductile damage in plates and rivets, i.e.: (*i*) the simplest LHM was adopted to capture post-necking stage in steel elements, (*ii*) monotonically decreasing triaxiality curves were considered based on the simplified expressions reported in [32] and (*iii*) linear DEC was used to model void coalescence (Fig. 16).

The adoption of these basic formulations was motivated by the necessity of accounting for the effects of hot-driving process [89,97,98].

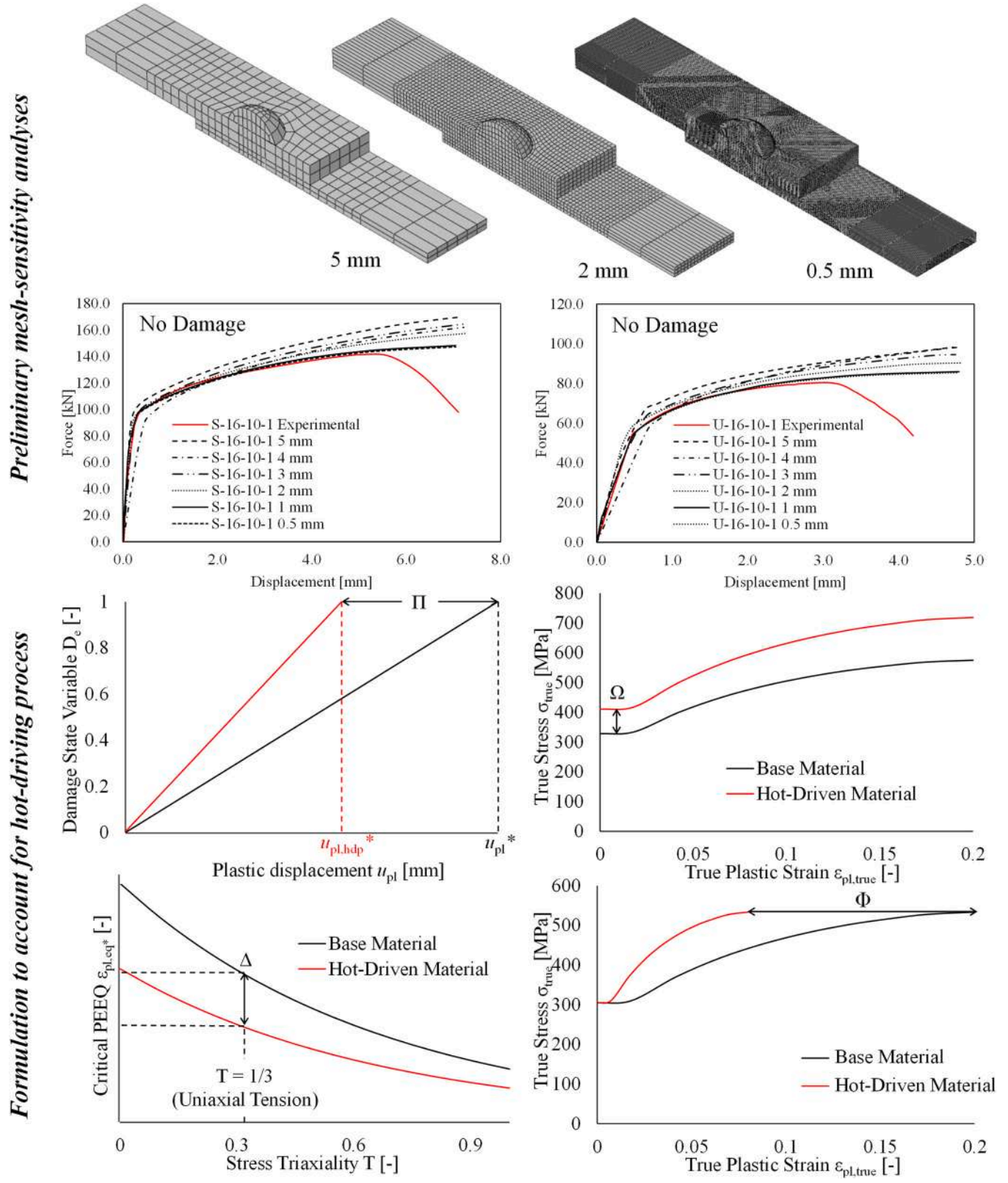

Fig. 16. Examples of application of reviewed damage models for structural purposes: monotonic failure of lap-shear hot-driven riveted connections. (Adapted from [89]).

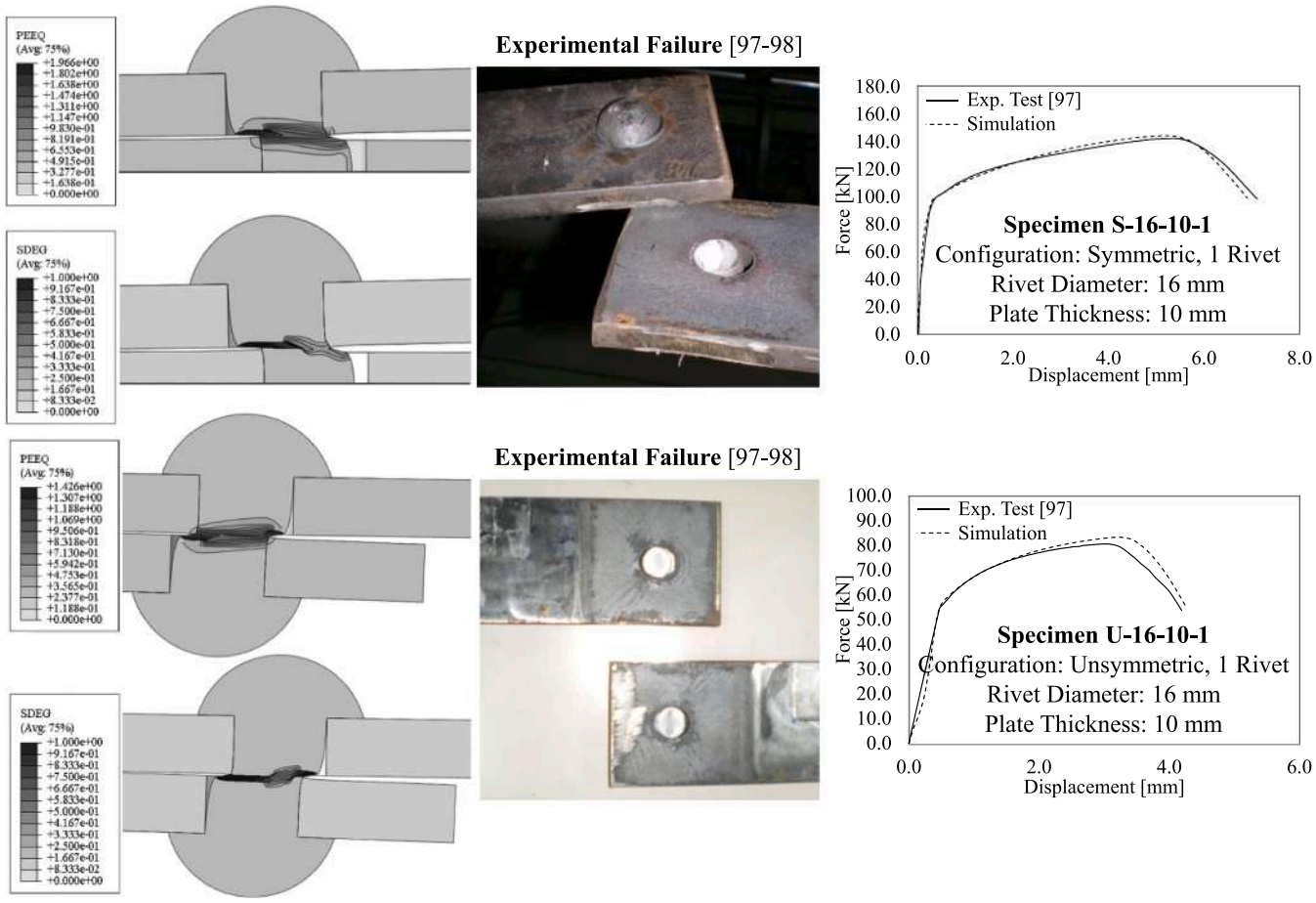

Fig. 16. (*continued*).

Namely, as claimed by several researchers [99–101], the combined action of hole drilling/punching and hot-driven hammering results in:

(a) an increase of rivet yield stress, i.e., modelled via the rivet overstrength ratio $\Omega = f_{y,hdp}/f_y$, [97,98];

(*b*) a reduction of plates ductility without significant yield stress variation, i.e., modelled through the ductility reduction ratio $\Phi = \varepsilon_{pl,true,u,hdp}/\varepsilon_{pl,true,u}$;.

(*c*) a sharp acceleration of damage in plates and rivets, i.e., modelled through the critical strain ratio $\Delta = \varepsilon_{pl,eq,hdp}^* / \varepsilon_{pl,eq}^*$ (GDDC) and the plastic displacement ratio $\Pi = u_{pl,hdp}^* / u_{pl}^*$ (DEC).

For the sake of clarity, in above expressions the subscript "hdp" refers to hot-driven material features.

It is worth remarking that, although the above phenomena have a thermomechanical nature, the assumption of temperature-depending damage criteria (e.g., Johnson-Cook model [59]) was deemed unfeasible, as (*i*) the exact conditions of hot-driving are extremely variable, as rivets were manually heated and hammered and (*ii*) calibration of altered material features can be only performed indirectly, as hot-driving creates a monolithic assembly between plates and rivets [89,97].

Moreover, even adopting the simplest post-necking and damage formulations, a rather fine mesh size ($s = 1$ mm in connected zone) was required to achieve satisfactory results.

Nevertheless, proposed modifications of mechanical criteria enabled a very effective calibration of numerical models, with FEAs very closely matching experimental results both in terms of PEEQ and damage distribution at failure and force-displacement curves (for the sake of brevity, only results referred to specimens S-16–10-1 and U-16–10-1 are reported). According to [89], an average increase of + 25 % in terms of rivets yield strength (f_y = 315 N/mm^2, $f_{y,hdp}$ = 397 N/mm^2 – mean values [89]) can be used for safety assessment purposes [89,97]. Contrariwise, connections' displacement capacity is strongly reduced by hot-driving ($\Phi = 0.54$, $\Delta = 0.21$, $\Pi = 0.65$ – mean values [98]).

With reference to high-strength steel structural assemblies, Liu et al. [90] recently carried out an experimental and numerical study addressing the tensile and compressive ultimate behaviour of welded square hollow section T-joints (Fig. 17) made of Q690 high-strength steel (f_y = 565 N/mm^2, f_u = 657 N/mm^2 – mean values [90]). In order to simulate post-necking behaviour of Q690 steel, a LPHM formulation was adopted, i.e., with a calibrated value of $w = 0.05$ being selected based on the iterative procedure described by Yang et al. [102]. A refined FEM of T-joints was hence developed, with a refined mesh size ($s = 1$ mm) being adopted in the connection zone based on preliminary sensitivity analyses depicted in Fig. 17. FEMs were hence used to *i*) interpretate 3 compression (SJ-1-X) + 3 tension (SJ-2-X) monotonic experimental tests and *ii*) carry out a parametric study to identify key parameters governing the response of high-strength steel hollow T-joints.

It is worth highlighting that, in a similar fashion to [79], Liu et al. a-posteriori identified the ultimate capacity of joints in FEAs based on recommendations from Madhup et al. [103], i.e., in correspondence of a chord face indentation/deformation equal to 0.03 times the joint width (0.03 × 100 mm = 3 mm). Nevertheless, a rather good agreement both in terms of force-displacement curves and deformed configuration can be still seen up to such displacement threshold in all cases (mean error of +4.9 % and +11.2 % among FEAs and tests in compression and tension, respectively). Local buckling and plasticization phenomena deriving from a T-stub mechanism are coherently predicted.

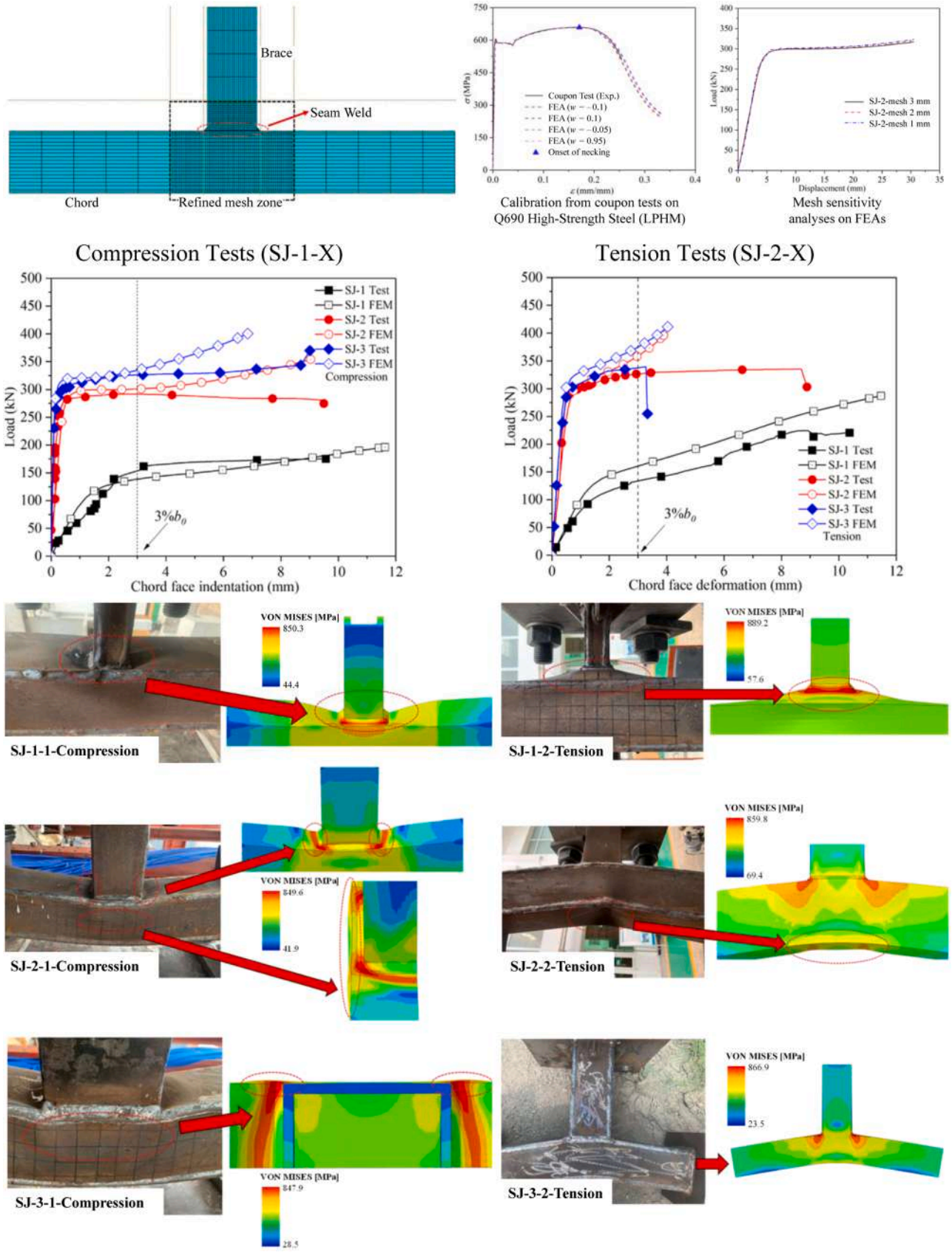

Fig. 17. Examples of application of reviewed damage models for structural purposes: tensile and compressive failure of hollow T-joints made of high-strength steel. (Adapted from [90]).

It can be still clearly observed that, when the DDS is reached, a fictious load increase is predicted by FEAs due to the absence of a DEC.

To this end, the interested reader may refer to the works of Cortese et al. [104] and Cheng et al. [105], which adopted a linear DEC (i.e., coupled with a HHM formulation and a T-ξ based GDDC) to assess the ultimate behaviour of notched high-strength steel coupons and bolted connections adopted in wind turbine towers, respectively. Moreover, in a similar fashion to [89], GDDC + DEC have been also successfully used by Wang et al. [106] to assess – with a purely mechanical formulation – the effect of progressive hydrogen embrittlement on the ductile burst behaviour of high-strength steel pipes.

In light of the above examples, the employment of post-necking and damage formulations can be deemed as very promising for practical engineering applications. Nevertheless, it is also very clear that an excessive computational effort would be required to assess the ultimate response of full-scale structures [107] (e.g., steel buildings equipped with bolted joints, diagonal braces, etc.) accounting for such refined formulations.

To this end, it is worth to mention that viable solutions are already common in practice to incorporate results from reviewed models in global FEMs such as the *sub-assembling* approach, i.e.:

- Introduction of refined and properly calibrated damage models in local FEMs accounting for the actual structural components' geometric and mechanical features;
- Derivation of equivalent indicators of the overall performance of the structural components of interest (e.g., force-displacement curves, moment-rotation curves, etc.);
- Calibration of simplified items able to account for non-linear response of details in global FEMs (e.g., lumped plastic hinges, non-linear spring elements, etc.);
- Assessment of the global non-linear behaviour of the entire structure by equivalently accounting for the components' response.

Some recent research works indeed adopted the above technique to balance analyses accuracy and computational effort while assessing the performance of large structures featuring complex components, e.g. Tartaglia et al. [108], which investigated the performance of an existing industrial steel warehouse accounting for brittle fracture of bolted truss connections, and Milone et al. [109], which accounted for damage and fracture of braces and moment-resisting joints in the global assessment of a multi-storey steel building designed before the entry in force of adequate seismic provisions in Italy.

7. Conclusive remarks

FEM is widely used by researchers and designers to address structural design and safety assessment of steel components and structures [1–6]. Nevertheless, up to recent times, very few provisions were available for a conscious and reliable use of numerical models in practice [13,14,17–19]. In light of new developments of the draft of prEN1993–1-14:2023 [23], which allows for advanced damage and fracture modelling of steel components, in the present work a review of consolidated post-necking and damage models was presented to serve as a guideline for both researchers and designers. Based on reviewed theoretical and applicative works, the following conclusive remarks can be pointed out:

1. Plastic behaviour of ductile metals such as structural steels can be ideally divided in two phases, i.e., plasticity-dominated stage (PDS) until necking and damage-dominated stage (DDS) until failure [30,33]. Nevertheless, widespread constant-volume equation for stress-strain curves are valid only in pre-necking stage. Therefore, post-necking formulations should be properly introduced and calibrated. Most popular models assume a linear (LHM) or exponential (HHM) evolution of true stresses after necking [33–36], although combined (LPHM) [33,39] or more complex [40–42] formulations have been proposed;
2. According to the reviewed documents [39,40,45,46], LPHM appears to show the highest accuracy, although an extra parameter (w) has to be iteratively calibrated. Nevertheless, while HMM proved to be largely conservative, LHM can still be used for practical purposes in light of its intrinsic simplicity, although being slightly unconservative in some cases;
3. In absence of damage, ductile steels would harden up to failure. Nevertheless, the presence of inclusions and second-phase particles induces void formation, growth and coalescence, resulting in material softening and fracture [48,53,54]. Therefore, proper damage initiation criteria should be introduced to account for such effect. The large majority of reviewed works are based on the seminal contribution of Rice & Tracey (RT Model [50]), which highlighted the key influence of stress triaxiality T on damage development in ductile materials. Among available formulations, void growth model (VGM) and stress-modified critical strain (SMCS) model [53,54] gained the highest popularity in light of their simplicity and consistency with physical evidences. Nevertheless, more generalized ductile damage criteria (GDDC) can be found in literature [58–62,64,66,69,92], e.g., either on analytical bases or in the form of so-called triaxiality curves;
4. Multiple studies highlighted some inconsistencies in RT Model, as the assumption of rigid-perfectly plastic material does not comply with steel monotonic behaviour. These issues were often overcome by introducing a material-depending triaxiality exponent β. Among modern formulations, SMCS is arguably the simplest option, although it may sometimes inaccurately capture the ductile fracture of specimens with complex cross-sections, i.e., due to its inability to account for variable stress histories up to failure. Contrariwise, while being more computationally onerous, VGM has improved accuracy and can be easily extended to cyclic conditions (CVGM [57]). With reference to triaxiality curves, multiple examples can be found in literature based on experimental tests [32,60,69]. Although more complex models accounting for shear sensitivity [61,67] have been proposed, their application appears exceedingly sophisticated for common structural applications;
5. Damage initiation criteria can be either intended to directly indicate failure or coupled with damage evolution criteria (DEC) to account for post-cracked residual stiffness of steel. Two main criteria can be found in literature, i.e. the simplest linear DEC [84] or the more complex exponential DEC [86], which in turn can be either defined through a displacement-based or an energy-based formulation [87]. Reviewed documents proved the effectiveness and good mesh-insensitivity of displacement-based linear DEC for structural steels, while more refined models may be suitable for other metallic alloys [86,87];
6. Three comprehensive applications of reviewed post-necking and damage formulations were presented, i.e., concerning the tensile fracture of high-strength bolts [88], the static failure of lap-shear hot-driven riveted connections [89] and the tensile/compressive failure of high-strength steel hollow T-joints [90]. As shown by the Authors, a conscious use of damage formulations – possibly extended to account for peculiar phenomena such as hot-driving process – can lead to reliable and accurate predictions of the structural performance of structural steel components and details.

CRediT authorship contribution statement

Aldo Milone: Writing – original draft, Visualization, Formal analysis, Data curation, Conceptualization. **Pietro Foti:** Writing – original draft, Visualization, Formal analysis, Data curation. **Filippo Berto:** Writing – review & editing, Supervision. **Raffaele Landolfo:** Writing – review & editing, Supervision.

Declaration of Competing Interest

The authors declare that they have no known competing financial interests or personal relationships that could have appeared to influence the work reported in this paper.

Data Availability

Data will be made available on request.

References

[1] Friswell MI, Mottershead JE. Finite element modelling. Solid Mech Its Appl 1995: 7–35.
[2] Jameson A. Re-engineering the design process through computation. 35th Aerosp Sci Meet Exhib 1997:97–0641.
[3] Huebner KH, Dewhirst DL, Smith DE, Byrom TG. The finite element method for engineers. New York, NY, USA: Wiley-Interscience; 2001.
[4] Khoury R, Harder DW. Numerical methods and modelling for engineering. Berlin, Germany: Springer; 2016.
[5] Rao RS. The finite element method in engineering. 6th edition..,. Oxford, UK: Butterworth-Heinemann; 2016.
[6] Kurowski PM. Finite element analysis for design engineers. 3rd edition. Warrendale, PA, USA: SAE International; 2023.
[7] Computer and Structures, Inc. SAP 2000 v.25 User's Manual. Walnut Creek, CA, USA: CSI; 2024.
[8] Seismosoft. Seismostruct v.22 User's Manual. Pavia, Italy: Seismosoft; 2022.
[9] Dassault. Abaqus 2023 User's Manual. lizy-Villacoublay, France: Dassault Systèmes Simulia Corp, Vé; 2023.
[10] Ansys Inc. Ansys Mechanical User's Guide. Canonsburg, PA, USA: Ansys Inc; 2021.
[11] Grätsch T, Bathe KJ. A posteriori error estimation techniques in practical finite element analysis. Comput Struct 2005;83:235–365.
[12] Schmidt H, Alber T, Wehner T, Blakytny R, Wilke HJ. Discretization error when using finite element models: analysis and evaluation of an underestimated problem. J Biomech 2009;42:1926–34.
[13] CEN. EN1993-1-5 – Eurocode 3: design of steel structures - Part 1-5: plated structural elements. Brussels, Belgium: CEN; 2006.
[14] CEN. EN1993-1-6 – Eurocode 3: Design of steel structures - Part 1-5: Strength and stability of shell structures. Brussels, Belgium: CEN; 2007.
[15] Kuhlmann U, Schmidt-Rasche C, Jörg F, Pourostad V, Spiegler J, Euler M. Update on the revision of Eurocode 3 – evolution by improvement and harmonization. Steel Constr 2021;14(1):2–13.
[16] Dunai L, Kövesdi B, Gardner L, Al-Emrani M, Casafont M, Degée H, Jandera M, Kuhlmann U, Taras A, Walport F. Design assisted by finite element analysis – Introduction to prEN 1993-1-14 and Technical Report. ce/Pap 2023;6(3-4): 2677–82.
[17] AISC. ANSI/AISC 360-16: specification for structural steel buildings. Chicago, IL, USA: AISC; 2016.
[18] ASME. ASME V&V10: standard for verification and validation in computational solid mechanics. New York, NY, USA: ASME; 2020.
[19] AWS. AWS A9.5-2013: guide for verification and validation in computation weld mechanics.. Doral, FL, USA: AWS; 2013.
[20] European Commission. M/515 EN: mandate for amending existing eurocodes and extending the scope of structural eurocodes – Ref. Ares(2012)1516834.. Brussel, Belgium: European Commission,; 2012.
[21] CEN/TC 250 (2013). Response to Mandate M/515 'Towards a second generation of EN Eurocodes' – Ref. N 993. CEN TC/250, Brussel, Belgium.
[22] European Commission (2022). Towards the publication of the Second Generation Eurocodes: the European Commission Mandate M/515 is now completed. Consulted Online (https:// eurocodes.jrc.ec.europa.eu/news/towards-publication-second-generation-eurocodes-european-commission-mandate-m515-now-completed).
[23] CEN. prEN1993-1-14:2023 – eurocode 3: design of steel structures – part 1-14: design assisted by finite element analysis (2023 Draft, subjected to CEN enquiry phase). Brussel, Belgium: CEN,; 2023.
[24] Garrison WM, Moody NR. Ductile fracture. J Phys Chem Solids 1987;48(11): 1035–74.
[25] Milne I, Ritchie RO, Karihaloo B. Comprehensive structural integrity. Amsterdam, Netherlands: Elsevier; 2003.
[26] Gulyaev AP. Ductile and brittle fracture of steel. Met Sci Heat Treat 1977;19(7): 618–9.
[27] Benzerga AA, Besson J, Pineau A. Anisotropic ductile fracture Part I: experiments. Acta Mater 2004;52:4623–38.
[28] Pineau A, Benzerga AA, Pardoen T. Failure of metals I: brittle and ductile fracture. Acta Mater 2016;107:424–83.
[29] Li H, Fu M. Deformation-based processing of materials: behavior. Performance, Modeling, and Control – Chapter 3: Damage Evolution and Ductile Fracture. Amsterdam, Netherlands: Elsevier,; 2019.
[30] Voyiadjis GZ, Kattan PI. A plasticity-damage theory for large deformation of solids - I. Theoretical formulation. Int J Eng Sci 1992;30(9):1089–108.
[31] Xin H, Veljkovic M, Correia JAFO, Berto F. Ductile fracture locus identification using mesoscale critical equivalent plastic strain. Fatigue Fract Eng Mater Struct 2021. https://doi.org/10.1111/ffe.13429.
[32] Yang F, Veljkovic M. Damage model calibration for S275 And S690 steels. ce/Pap 2019;3(5-6):262–71.
[33] Tu S, Ren X, He J, Zhang Z. Stress–strain curves of metallic materials and post-necking strain hardening characterization: a review. Fatigue Fract Eng Mater Struct 2019;43:3–19.
[34] Considère A. Ann Des Ponts Et Chauss– 1885;9:574.
[35] Hollomom JH. Tensile deformation. Trans Metall Soc AIME 1945;162:268–90.
[36] Callister Jr WD. Fundamentals of materials science and engineering. 2nd edition.,. John Furkan & Sons; 2005. ISBN 978-0-471-47014-4.
[37] Swift HW. Plastic instability under plane stress. J Mech Phys Solids 1952;1:1–18.
[38] Cao J, Li F-G, Ma X-K, Sun Z-K. Tensile stress−strain behavior of metallic alloys. Trans Nonferrous Met Soc China 2017;27:2443–53.
[39] Ling Y. Uniaxial true stress-strain after necking. AMP J Technol 1996;5(1):37–48.
[40] Wang Y, Xu S, Ren S, Wang H. An experimental-numerical combined method to determine the true constitutive relation of tensile specimens after necking. Adv Civ Eng 2016:6015752.
[41] Voce E. The relationship between stress and strain for homogeneous deformation. J Inst Met 1948;74:537–62.
[42] Pham QT, Kim Y-S. Evaluation on flexibility of phenomenological hardening law for automotive sheet metals. Metals 2022;12(4):578.
[43] Ramberg W, Osgood WR. Description of stress-strain curves by three parameters. Technical Note No. 902. Washington DC: National Advisory Committee for Aeronautics; 1943.
[44] CEN. EN1993-1-1 – eurocode 3: design of steel structures – part 1-1: general rules and rules for buildings. Brussels, Belgium: CEN; 2022.
[45] Dhar S, Sethuraman R, Dixit PM. A continuum damage mechanics model for void growth aad micro crack initiation. Eng Fract Mech 1996;53(6):917–28.
[46] Cabezas EE, Celentano DJ. Experimental and numerical analysis of the tensile test using sheet specimens. Mecánica Comput 2002;21:854–73.
[47] Le Roy G, Embury JD, Edward G, Ashby MF. A model of ductile fracture based on the nucleation and growth of voids. Acta Metall 1981;29:1509–22.
[48] Anderson TL. Fracture Mechanics: Fundamentals and Applications. 4th edition. CRC Press, Taylor & Francis Group; 2017.
[49] McClintock FA. A criterion for ductile fracture by the growth of holes. J Appl Mech 1968;35(2):363–71.
[50] Rice JR, Tracey DM. On the ductile enlargement of voids in triaxial stress fields. J Mech Phys Solids 1969;17:201–17.
[51] Von Mises R. Mechanik der festen Körper im plastisch-deformablen Zustand. Nachr Von der Ges der Wiss zu Göttingen Math-Phys Kl 1913;1:582–92 (In German).
[52] Hencky H. Zur Theorie plastischer Deformationen und der hierdurch im Material hervorgerufenen Nachspannngen. Z Angew Math Mech 1924;4(4):323–34 (In German).
[53] Kanvinde AM, Deierlein GG. The void growth model and the stress modified critical strain model to predict ductile fracture in structural steels. J Struct Eng 2006;132:1–52.
[54] Rousselier G. Ductile fracture models and their potential in local approach of fracture. Nucl Eng Des 1987;105(1):113–20.
[55] Kanvinde A, Deierlein GG. Micromechanical simulation of earthquake induced fractures in steel structures. Blume Center Technical Report no. 145. Stanford, CA: Stanford University,; 2004.
[56] Hancock JW, Mackenzie AC. On the mechanisms of ductile failure in high-strength steels subjected to multi-axial stress-states. J Mech Phys Solids 1976;24 (2-3):147–60.
[57] Kanvinde AM, Deierlein GG. Cyclic void growth model to assess ductile fracture initiation in structural steels due to ultra low cycle fatigue. J Eng Mech 2007;133 (6):701–12.
[58] Jia LJ, Kuwamura H. Ductile fracture simulation of structural steels under monotonic tension. J Struct Eng (ASCE) 2014;04013115.
[59] Johnson GR, Cook WH. Fracture characteristics of three metals subjected to various strains, strain rates, temperatures and pressures. Eng Fract Mech 1985;21 (1):31–48.
[60] Bonora N. A nonlinear CDM model for ductile failure. Eng Fract Mech 1997;58 (1):11–28.
[61] Korgesaar M. The effect of low stress triaxialities and deformation paths on ductile fracture simulations of large shell structure. Mar Struct 2019;63:45–64.
[62] Mirone G, Barbagallo R, Corallo D. A new yield criteria including the effect of lode angle and stress triaxiality. Procedia Struct Integr 2016;2:3684–96.
[63] Lode W. Versuche über den Einfuss der mittleren Hauptspannung auf das Fliessen der Metalle Eisen Kupfer und Nickel. Ztg Phys 1926;36:913–39 (In German).
[64] Malcher L, Andrade Pires FM, César de Sá JMA. An extended GTN model for ductile fracture under high and low stress triaxiality. Int J Plast 2014;54: 193–228.
[65] Irgens F. Continuum mechanics. Springer Berlin, Heidelberg; 2008.
[66] Erice B, Galvez F. A coupled elastoplastic-damage constitutive model with Lode angle dependent failure criterion. Int J Solids Struct 2014;51:93–110.
[67] Hooputra H, Gese H, Dell H, Werner H. A comprehensive failure model for crashworthiness simulation of aluminium extrusions. Int J Crashwortiness 2004;9 (5):449–64.
[68] Di Lorenzo G, Formisano A, Terracciano G, Landolfo R. Iron alloys and structural steels from XIX century until today: evolution of mechanical properties and proposal of a rapid identification method. Constr Build Mater 2021;302:124132.

[69] Ohno N. Material models of cyclic plasticity with extended isotropic hardening: a review. Mech Eng Rev 2015;2(1):14-00425.
[70] De Angelis F. A comparative analysis of linear and nonlinear kinematic hardening rules in computational elastoplasticity. Technische Mechanik 2011;32(2-5): 164–73.
[71] Dutta A, Dhar S, Acharyya SK. Material characterization of SS 316 in low cycle fatigue loading. J Mater Sci 2010;45:1782–9.
[72] Tai WH. Plastic damage and ductile fracture in mild steels. Eng Fract Mech 1990; 37(4):853–80.
[73] Sun YQ, Detraux JM, Touot G, Francois D. Mecanisme de la rupture ductile dans la a graphite spheroidal ferritique. Mem Et Etudes Sci Rev De Metall 1983:183–95 (In French).
[74] Beremin FM. Study of the fracture criterion for ductule rupture of A508 steel. Procedia ICF5 Congr 1981:809–16.
[75] Barnby JT, Shi YW, Nadkarni AS. On the void growth in C-Mn structural steel during plastic deformation. Int J Fract 1984;25:271–84.
[76] Shockey DA, Dao KC, Seaman L, Curran DR. Computational modelling of microstructural fracture processes in A533B pressure vessel steel. NP-1398 Final Report. EPRI; 1980.
[77] Brownrigg A, Spitzig WA, Richmond O, Embury JD. The influence of hydrostatic pressure on the flow stress and ductility of a spherodized 1045 steel. Acta Metall 1983;31:1141–50.
[78] Kiran R, Khandelwal K. Experimental studies and models for ductile fracture in ASTM A992 steels at high triaxiality. J Struct Eng (ASCE) 2014;140(2):04013044.
[79] Tartaglia R, Milone A, D'Aniello M, Landolfo R. Retrofit of non-code conforming moment resisting beam-to-column joints: a case study. J Constr Steel Res 2022; 189:107095.
[80] Moradnezhad F, Zeinoddini M, Fanaie N, Moghaddam H, Khanmohammadi M, Zandi AP, Hussaini SA, Rezaeinejad H, Kazemzadeh O. A novel ductile CHS knee bracing system for rehabilitation of earthquake-damaged buildings: the case of Sarpol-e-Zahab (Iran) earthquake. J Build Eng 2023;65:105748.
[81] Kuwamura H, Yamamoto K. Ductile crack as trigger of brittle fracture in steel. J Struct Eng (ASCE) 1997;123(6(729)):729–35.
[82] Arita M, Iyama J. Fundamental verification of crack extension rule to estimate fracture of steel. Summ Tech Pap Annu Meet AIJ 2009;20137:273–4 (in Japanese).
[83] Miller DK. Lesson learned from the Northridge Earthquake. Eng Struct 1998;20(4-6):249–60.
[84] Hillerborg A, Modeer M, Petersson PE. Analysis of crack formation and crack growth in concrete by means of fracture mechanics and finite elements. Cem Concr Res 1976;6(6):773–81.
[85] Cook RD. Finite element modelling for stress analysis. New York: J Wiley; 1995.
[86] Qu RT, Zhang ZJ, Zhang P, Liu ZQ, Zhang ZF. Generalized energy failure criterion. Sci Rep 2016;6:23359.
[87] Ammar MMA, Shirinzadeh B, Elgamal H, Nasr MNA. On the role of damage evolution in finite element modeling of the cutting process and sensing residual stresses. Sensors 2022;22:8547.
[88] Yang F, Veljkovic M, Cheng L. Fracture simulation of fully and partially threaded bolts under tension. ce/Pap 2021;4(2-4):156–61.
[89] Milone A, D'Aniello M, Landolfo R. Influence of camming imperfections on the resistance of lap shear riveted connections. J Constr Steel Res 2023;203:107833.
[90] Liu S, Chen S, Wang W, Zhou Z. Experimental and analytical study of grade Q690 high-strength steel square hollow section T joints under axial tension and compression. Structures 2024;64:106486.
[91] Grimsmo EL, Aalberg A, Langseth M, Clausen AH. Failure modes of bolt and nut assemblies under tensile loading. J Constr Steel Res 2016;126:15–25.
[92] Bao Y, Wierzbicki T. On fracture locus in the equivalent strain and stress triaxiality space. Int J Mech Sci 2004;46(1):81–98.
[93] Willms R. High strength steel for steel constructions. Proc 11th Nord Steel Constr Conf 2009;181:597–604.
[94] Pyshmintsev IY, Pumpyanskii DA, Farber VM. Ductility of steel and its characteristics. Met Sci Heat Treat 2007;49(11-12):519–25.
[95] Collette Q, Wouters I, Lariks L. Evolution of historical riveted connections: joining typologies, installation techniques and calculation methods. Struct Repairs Maint Herit Archit XII 2011;118:295–306.
[96] Vermes WJ. Design and performance of riveted bridge connections. Columbus, OH, USA: Ohio Transportation Engineering Conference; 2007.
[97] D'Aniello M, Portioli F, Fiorino L, Landolfo R. Experimental investigation on shear behaviour of riveted connections in steel structures. Eng Struct 2011;32(2): 516–31.
[98] Milone A. PhD Thesis. Perform Lap-Shear Hot-Driven Riveted Connect: Exp Numer Study 2023.
[99] Hechtman RA. A study of the effects of heating and driving conditions on hot-driven structural steel rivets. Urbana-Champaign, IL, USA: University of Illinois; 1948.
[100] Munse WH, Cox HC. The static strength of rivets subjected to combined tension and shear. Eng Exp Station 1956;Bulletin no. 437.
[101] Kulak GL, Fisher JW, Struik JHA. Guide to design criteria for bolted and riveted joints. 2nd edition..,. Hoboken, NJ, USA: John Wiley & Sons; 1987.
[102] Yang F, Veljkovic M, Liu Y. Ductile damage model calibration for high-strength structural steels. Constr Build Mater 2020;263:120632.
[103] Madhup P, Young B. Tests of cold-formed high strength steel tubular T-joints. Thin-Walled Struct 2019;143:106200.
[104] Cortese L, Coppola T, Campanelli F, Broggiato GB. A J2–J3 approach in plastic and damage description of ductile materials. Int J Damage Mech 2016;25(2): 228–50.
[105] Cheng L, Yang F, Seidel M, Veljkovic M. FE-assisted investigation for mechanical behaviour of connections in offshore wind turbine towers. Eng Struct 2023;285: 116039.
[106] Wang H, Wang T, Yang S, Gao J, Yu Y, Tao H. Ductile burst behavior of high pressure X100 steel pipe considering hydrogen damage. Int J Hydrog Energy 2024;58:362–79.
[107] Fincato R, Tsutsumi S. Ductile fracture modeling of metallic materials: a short review. Frat e Integrità Strutt 2022;(59):1–17.
[108] Tartaglia R, Milone A, Prota A, Landolfo R. Seismic retrofitting of existing industrial steel buildings: a case-study. Materials 2022;15(9):3276.
[109] Milone A, Tartaglia R, D'Aniello M, Landolfo R. Seismic upgrade of a non-code compliant multi-storey steel building: a case study. J Build Eng 2024;95:110151.